J. Membrane Biol. 21, 197–259 (1975)

Nitrogenous Cations as Probes of Permeation Channels

Julio H. Moreno* and Jared M. Diamond

Physiology Department, UCLA Medical School, Los Angeles, California 90024

Received 19 August 1974; revised 2 January 1975

Summary. Nitrogenous cations may provide information-rich probes of cation-selective channels. Hence, for 52 nitrogenous cations we have used dilution potentials and biionic potentials to measure relative permeability coefficients (P's) across gallbladder epithelia of frog and rabbit, and have also determined the free-solution mobilities. Measured P's of most cations are uninfluenced by the presence of the neutral form. The main permeation pathway for most hydrophilic cations is across the tight junctions. P's decrease with molecular size and increase with number of donor protons available for hydrogen-bond formation. Selectivity isotherms have been constructed from variation in P's due to pH or due to differences among individual animals. Both types of variation are consistent with the pattern expected from variation in electrostatic field strength of cation-binding sites. The isotherms permit P's to be re-expressed in a way that largely eliminates effects of species differences in field strength. Remaining species differences in P's are well fitted by a model of steric restriction, provided that one takes into account the effect of hydrogen bonding on molecular size. Rabbit gallbladder behaves as if it has narrower permeation channels than frog gallbladder. After correction for these steric effects, P is found to increase with number of donor protons n_H up to four protons, with a steeper slope in rabbit than in frog gallbladder, but is independent of n_H from four to at least nine. Two groups of cations appear to permeate significantly via pathways other than tight junctions: oxycations, via polar pathways in epithelial cell membranes of rabbit but not frog gallbladder; and lipid-soluble cations, via membrane lipid.

The results suggest that the cation-binding sites of gallbladder tight junction are acidic proton-acceptors that discriminate more sharply among proton donors than does water. Proton-rich solutes tend to be more permeant for two reasons: stronger binding energies to membrane proton-acceptor sites, and smaller effective size in a proton-acceptor environment. As deduced from comparisons of nitrogenous cation selectivity patterns, the permeation channel through gallbladder tight junction differs from nerve's sodium channel and artificial carriers and channels in its higher hydration and lower range of selectivity. Based on the steric analysis of nitrogenous cation permeation, one can correct alkali cation permeability coefficients for the effect of steric restriction.

It has often been shown that monovalent organic cations or nitrogenous bases may be effective in processes which were previously thought

* *Present address:* Instituto de Biología Celular, Facultad de Medicina, Universidad de Buenos Aires, Paraguay 2155, Buenos Aires, Argentina.

highly specific for the alkali cations. Some examples are that: several nitrogenous cations are nearly as effective as Na^+ in carrying current through the Na^+ channel of nerve (Lorente de Nó, Vidal & Larramendi, 1957; Hille, 1971) and acetylcholine-activated end-plate channels (Maeno, 1974); the tetraethylammonium cation blocks the K^+ channel of nerve (Tasaki & Hagiwara, 1957; Armstrong & Binstock, 1965; Hille, 1967); glass electrodes (Eisenman, 1965*a*, Fig. 39) and macrocyclic carriers (Eisenman & Krasne, 1973) selective for alkali cations also respond to some nitrogenous cations; NH_4^+ and the alkali cations share the same permeation pathway through gallbladder tight junctions (Moreno & Diamond, 1973*a*, 1974*b*, 1975); the organic cation 2,4,6-triaminopyrimidinium blocks the cation permeation through the gallbladder tight junctions (Moreno, 1974); and some nitrogenous cations may replace alkali cations in specific stimulatory or inhibitory effects on enzymes (Eisenman & Krasne, 1974).

These nitrogenous cation effects may prove useful probes for analyzing the molecular structure of alkali cation permeation channels, because nitrogenous cations are far more numerous and varied than are metallic cations. Pioneer efforts in this direction have been studies of cation permeation through the Na^+ channel of nerve by Hille (1971), and of cation conductances of bilayers doped with macrocyclic carriers by Eisenman and Krasne (1973). Nitrogenous cation studies may also prove relevant to understanding permeation of nonelectrolytes through pores, since both groups of solutes have similar chemical groups and some similar modes of interaction. The net charge of the cations, however, makes their permeability far easier to measure (by electrical techniques).

That nitrogenous cations provide information-rich probes is in theory their potential virtue but has in practice been their weakness. Their interactions with membrane sites are likely to depend on many factors – especially on hydrogen bonds, steric effects, coordination number, coulomb forces, and hydration. Thus, interpretation of their permeability patterns proves to be a complex and difficult task. Furthermore, some physical parameters whose values are needed if one is to interpret measured permeability coefficients, such as free-solution mobility and molecular dimensions, have apparently not been measured for most nitrogenous cations of physiological interest.

In the present paper we develop methods by which the contributions of the above-mentioned factors to nitrogenous cation selectivity may be partially sorted out, and we apply these methods to probing the permeation channel of gallbladder tight junction. In addition, we present measurements of free-solution mobilities (Appendix) and molecular dimensions (Table 5).

Preliminary accounts of one aspect of these results have appeared (Moreno & Diamond, 1973*b*, 1974*a*). Advantages of gallbladder for such a study include its durability, relative ease of permeability measurement that it permits, and accumulated information about its permeation channel derived from studies of alkali cations (Wright & Diamond, 1968; Barry, Diamond & Wright, 1971; Moreno & Diamond, 1973*a*, 1974*b*, 1975). A further important advantage proves to be a range of selectivity wide enough to be interesting but narrow enough that permeabilities of many cations can be accurately measured. The much wider range of selectivity exhibited by macrocyclic carriers and nerve's Na^+ and K^+ channel makes measurements on some cations difficult or impossible in these systems, because of interference from contamination with traces of highly permeant NH_4^+ or K^+ in the former case and because of undetectably low permeabilities in the latter case.

As background, it may be recalled that the main route of cation permeation across gallbladder epithelium is via the misnamed tight junctions between the cells, not via the epithelial cell membranes themselves (Frömter, 1972; Frömter & Diamond, 1972). However, ion permeation through tight junctions and through pores in cell membranes may be quite similar. Evidence derived from the alkali cation studies cited above suggests that the permeation channel through gallbladder tight junction is relatively hydrated and roughly 10–20 Å in diameter depending on the animal species, that the sites controlling cation permeation behave as acidic groups with a pK_a value near 4.5, and that alkali cation selectivity depends on the field strength of the sites and on steric effects in the channels (for a review *see* Moreno & Diamond, 1975).

Materials and Methods

Experimental Techniques

Gallbladders were used from New Zealand white rabbits weighing ca. 3 kg and from bullfrogs (*Rana catesbiana*) weighing ca. 350 g. No differences were noticed among gallbladders from animals of different sexes. Methods for measuring relative permeability coefficients of ions (abbreviated *P*'s) across gallbladder *in vitro* were in general similar to those described previously (Moreno & Diamond, 1974*b*). Briefly, the gallbladder was removed from an animal, washed free of bile and cut open, and a piece of tissue was mounted in a window of 20 mm^2 area between chambers stirred by magnetic bars. Permeability coefficients were calculated (*see* p. 202) from dilution potentials and biionic potentials resulting from ion concentration gradients across the gallbladder. The permeability characteristics of the gallbladder are symmetrical—i.e., reversing the bathing solutions reverses the observed electrical potential difference or p.d. (Diamond, 1962; Barry & Diamond, 1970; Moreno & Diamond, 1974*b*). P.d.'s other than diffusion poten-

tials, such as p.d.'s arising from active transport of ions, are negligible under the experimental conditions used. Unless otherwise noted, the experimental temperature was 23 ± 1 °C.

Electrodes

In most experiments we used Ag–AgCl electrodes, prepared as described previously (Moreno & Diamond, 1974*b*). If the asymmetry potential measured with both electrodes in the same 150 mM salt solution exceeded 0.2 mV, the electrodes were rejected. When the gallbladder separated solutions with differing Cl^- concentrations, we subtracted from measured p.d.'s the electrode potential, calculated as

$$V'' - V' = (RT/F) \ln (a'_{Cl}/a''_{Cl}) \quad (1)$$

where $V'' - V'$ is voltage (mV), a is activity, superscripts $'$ and $''$ represent the two bathing solutions, and R, T and F have their usual meanings. In a few experiments the p.d. was measured simultaneously with Ag–AgCl electrodes [correcting for electrode potentials by Eq. (1)] and with 150 mM NaCl bridges immobilized by 4% agar (correcting for junction potentials as described by Barry & Diamond, 1970). The two measurements were found to agree within 0.2 mV.

Solutions

The composition (in millimolal units) of the standard solution used was: 150 mM Na^+, 150.5 Cl^-, 0.25 Ca^{++}, 5 K^+, and 3 $H_2PO_4^- - HPO_4^{2-}$, adjusted to pH 7.0. To obtain pH 5.0, the phosphate buffer was replaced by 1.77 mM $H_2PO_4^-$ and 3.2 mM phthalate. NaCl was replaced by 150 mM KCl to obtain a test solution of the latter salt. To measure dilution potentials, (NaCl) in the standard solution was reduced to 75 mM by isosmotic replacement with mannitol.

Test solutions of nitrogenous cations were generally prepared by replacing Na^+ with the test cations at 150 mM. (The sole exceptions were in the cases of dibutylamine, diisobutylamine, heptylamine, and tributylamine, which are insoluble or poorly soluble at this concentration. These four cations were studied at 100 mM, and the three other solutions mentioned in the preceding paragraph for use in measuring biionic potentials or dilution potentials were correspondingly changed from 150 to 100 mM NaCl, from 150 to 100 mM KCl, and from 75 to 50 mM NaCl.) Two different procedures were used for preparing the solutions, depending on whether the cation was commercially supplied as the chloride salt or as the neutral amine. In the former case, since some of the salts are highly hygroscopic, we initially prepared a solution by weighing the salt, then checked its concentration by potentiometric titration of Cl^- (Sanderson, 1952), and accordingly adjusted the final amount of water added. In the latter case, after preparing an initial solution by weighing the amine, we titrated with 200 mM HCl to the desired pH (7.0 or 5.0). Since the pH was chosen so that the pK_a of the amine would be considerably above the solution pH (usually by at least 2–4 pH units), the amount of HCl used for titration provided a check on the concentrations of the amine as assumed from weighing. In some instances Cl^- was then determined by potentiometric titration as an additional check. Osmolarity was also checked for some solutions. Solutions were usually prepared the day before an experiment, stored in a refrigerator, and used within five days.

The following cations were tested. In this list the cations supplied as the chloride salt are designated by "HCl", while the other cations were supplied as neutral amines: hydrazine, hydroxylamine · HCl, methylhydrazine, triaminoguanidine · HCl, aminoguanidine · HNO_3, ethylamine · HCl, dimethylamine · HCl, ethanolamine, *n*-propylamine, isopropylamine, allylamine, methylethylamine · HCl, methoxyethylamine,

2-aminopropanol, 3-aminopropanol, imidazole, *n*-butylamine, isobutylamine, sec-butylamine, *t*-butylamine, diethylamine, tetramethylammonium chloride, aminotrihydroxymethylmethane, 2-aminobutanol, *n*-pentylamine, *t*-pentylamine, *n*-hexylamine, dipropylamine, triethylamine, cyclohexylamine, benzylamine, *n*-heptylamine, dibutylamine, diisobutylamine, tripropylamine, tetraethylammonium chloride (all from Eastman Organic Chemicals, Rochester, New York); ethylenediamine, aminoethanethiol · HCl, 1-aminoethanol, isopentylamine, 6-aminohexanol, tributylamine (from Aldrich Chemical Co., San Leandro, California); ammonium chloride, choline chloride (Baker Chemical Co., Phillipsburg, New Jersey); methylamine · HCl, formamidine · HCl, guanidine · HCl, methylguanidine · HCl, trimethylamine · HCl, 5-aminopentanol · HCl (from Sigma Chemical Co., St. Louis, Missouri); methylhydroxylamine · HCl, acetamidine · HCl, azirane · HCl (ICN–K & K Laboratories, Irvine, California); biguanidine (Pfaltz and Bauer, Flushing, New York). Solutes were used as supplied by the manufacturer, without additional purification. Any contaminants present must have been at low concentration, since concentrations calculated from potentiometric titration, HCl titration, osmolarity, and weight generally agreed within 3% and since pK_a values estimated from HCl titration agreed with published values where available. The only exceptions were: (1) A sample of biguanidine that yielded an opaque solution and unexpected HCl titration curve. This sample was discarded in favor of a sample with expected behavior from another manufacturer, the one listed above. (2) An evidently impure sample of *t*-pentylamine, for which no purer source could be found and which was therefore not studied further. (3) A sample of 1-amino-1-ethanol, which evidently decomposed rapidly ($H_3C-C(NH_3^+)-OH \rightarrow NH_4^+ + H_3C-C(H)=O$) and was not studied further.

Throughout this paper, cations with a dissociable proton will be referred to by the simpler name of the corresponding amine; e.g., hydrazine instead of hydrazinium. We shall show that for all cations studied except perhaps $HO-NH_3^+$ and $HO-NH_2^+-CH_3$, the pK_a was sufficiently far above the experimental pH that the concentration of the neutral form was too low to affect the measured permeability of the charged form (pp. 205–207).

Experimental Protocol

The bathing solution on the side of the gallbladder facing the outside (the bloodstream) in the animal is called the serosal solution, while the bathing solution on the side facing the lumen in the animal is called the mucosal solution. Since the unstirred layer is thicker on the serosal side because of the connective tissue present (Diamond, 1966), all changes in solution composition to produce ion concentration gradients across the gallbladder were made on the mucosal side. The serosal solution was always the standard 150 mM NaCl solution and was renewed after each two or three changes of mucosal solution composition. The mucosal solution was changed from 150 mM NaCl to 75 mM NaCl and back to 150 mM NaCl to record the 2:1 NaCl dilution potential, and from 150 mM NaCl to 150 mM KCl or 150 mM *X*Cl and back to 150 mM NaCl to record the K^+/Na^+ or X^+/Na^+ biionic potential (abbreviating nitrogenous cations as X^+). The 2:1 NaCl dilution potential was measured after every second or third X^+/Na^+ biionic measurement, and the K^+/Na^+ biionic potential was measured after every second NaCl dilution potential measurement. These measurements not only served as a check on the condition of the preparation and possible effects of amines on permselectivity, but were also necessary to monitor any possible changes in the relative permeability coefficients P_K/P_{Na} or P_{Cl}/P_{Na}, which enter into the calculations of P_X/P_{Na} (*see* Eq. (2) below). In a given series of measurements, all solutions were at the same pH (7.0, 5.0 or 3.8).

Usually the permeabilities of a series of 6 to 12 cations were compared in the same gallbladder, usually twice, sometimes three times. There were no systematic differences

in P_X/P_{Na} (after correction for a leakage pathway: *see below*) with time after dissection. When P_X/P_{Na} for a given cation was measured repeatedly throughout an experiment, the coefficient of variation was on the average 5.5%. To reduce effects of individual variation among animals, chemically similar cations to be compared were studied in the same gallbladders. Unless specifically stated otherwise, errors are expressed as standard errors of the mean.

Calculations and Corrections for a Leakage Pathway

Relative permeability coefficients P_X/P_{Cl} were calculated from observed p.d.'s as described previously (Moreno & Diamond, 1974*b*). Briefly, we first calculated P_X/P_{Cl}, uncorrected for a leakage pathway, from the Goldman-Hodgkin-Katz equation:

$$V''-V'=(RT/F)\ln\frac{\Sigma P_M\gamma'_M(M)'+P_{Cl}\gamma''_{Cl}(Cl)''}{\Sigma P_M\gamma''_M(M)''+P_{Cl}\gamma'_{Cl}(Cl)'} \tag{2}$$

where P_i is the relative permeability coefficient of ion i, γ'_i or γ''_i is the ion's activity coefficient in bathing solution $'$ or $''$, quantities in parentheses are concentrations, M stands for any cation, the summation is taken over all cations present (Na^+, K^+, and the test cation X^+) and other symbols are as defined on p. 200. Since γ for the chloride salts of most test cations at the experimental temperature and concentrations is unknown, we assumed[1] γ_{XCl} equal to γ_{NaCl} at the same temperature and concentration as tabulated by Robinson and Stokes (1970), and we made the Guggenheim assumption that $\gamma_{X^+}=\gamma_{Cl^-}$. P_{Na}/P_{Cl} and P_K/P_{Cl} were calculated from the values of the NaCl dilution potential and the K^+/Na^+ biionic potential. These ratios were then combined with the value of the X^+/Na^+ biionic potential to obtain P_X/P_{Cl}. Cation-to-cation permeability ratios $(P_X/P_Y)_m$ corrected for leakage pathway were then calculated from the expression

$$(P_X/P_Y)_m=\frac{(P_X/P_{Cl})-(u_X/u_{Cl})}{(P_Y/P_{Cl})-(u_Y/u_{Cl})}. \tag{3}$$

In Eq. (3) the values of (P_X/P_{Cl}) and (P_Y/P_{Cl}) were those obtained from Eq. (2), while values of the free-solution mobility ratios (u_X/u_{Cl}) and (u_Y/u_{Cl}) were measured experimentally at 25°C (*see* Appendix).

The assumption underlying the leakage correction of Eq. (3) is that the measured transepithelial conductance G of gallbladder arises partly from selective channels which are virtually impermeable to anions, partly from a free-solution shunt that contains all the measured anion conductance. Evidence for this interpretation presented elsewhere (Barry *et al.*, 1971; Moreno & Diamond, 1974*b*, 1975; Moreno, 1975*a*, *b*) may be summarized as follows, and further new evidence will be presented on pp. 203–205.

---

1 Five types of evidence show that little error is introduced by this assumption. (a) The known value of $\gamma_{NH_4^+}$ is only 1.7% below that of γ_{NaCl} at 150 mM, 25°C (Robinson & Stokes, 1970). (b) γ's of Na^+ formate, acetate, propionate, and butyrate are 0–4% greater than that of γ_{NaCl} at 150 mM, 25°C (Robinson & Stokes, 1970). (c) For $H_3C-CH_2-NH_3^+Cl^-$ and $H_3C(CH_2)_5NH_3^+Cl^-$ the mobility ratio u_X/u_{Cl}, calculated from junction potentials on the assumption of $\gamma_{XCl}=\gamma_{NaCl}$, equals u_X/u_{Cl} calculated from conductance measurements, within an accuracy of 0.3 and 1.1%, respectively (Appendix). (d) Measured values of γ for $(CH_3)_4N^+Cl^-$, $(C_2H_5)_4N^+Cl^-$, $(C_3H_7)_4N^+Cl^-$, and $(C_4H_9)_4^+Cl^-$ interpolated to 150 mM all fall within a range of 1.8% of the average γ for all four salts (Lindenbaum & Boyd, 1964). (e) Values of γ at 100 mM and 25°C for nine of the cations used in our study, calculated from the Debye-Hückel equation, all fall within 3% of the value for Na^+ (Kielland, 1937).

(a) The chloride conductance G_{Cl} of a freshly dissected gallbladder is negligible. (b) Increases in G and in P_{Cl}/P_{Na} after dissection show that increases in the partial conductances G_{Cl} and G_{Na} are in the ratio of the free-solution mobilities u_{Cl} and u_{Na}. (c) Apparent changes in cation-to-cation permeability ratios with time after dissection disappear, if the ratios are corrected for a free-solution leakage pathway whose conductance is estimated from the measured G_{Cl}. (d) The Q_{10} of G_{Cl} in gallbladder does not differ significantly from the Q_{10} of Cl^- conductance in free solution, whereas the Q_{10} of G_{Na} is considerably higher. (e) Effects of pH on G_{Na} and G_{Cl} suggest that Cl^- and Na^+ permeate via separate channels. (f) 2,4,6-triaminopyrimidinium almost completely blocks G_{Na} without affecting G_{Cl}, and thereby causes gallbladder permeability properties to become similar to those of a free-solution pathway.

The time-dependent increase in leakage conductance in the experiments of Barry *et al.* (1971) has proved to be due to the absence of K^+ and phosphate from their bathing solutions (Moreno & Diamond, 1974*b*). In our experiments all solutions contained K^+ and phosphate, hence P_{Cl}/P_{Na} remained low and constant for many hours. For most cations the correction to P_X/P_{Na} introduced by Eq. (3) is very small, since $P_X/P_{Cl} \gg u_X/u_{Cl}$ and $P_{Na}/P_{Cl} \gg u_{Na}/u_{Cl}$. The lower the cation's permeability in native gallbladder and the higher the leakage conductance, the more important does the correction of Eq. (3) become. For instance, consider the relatively impermeant cation tetramethylammonium [$(CH_3)_4N^+$, abbreviated TMA], for which $u_{TMA}/u_{Cl}=0.46$ and the measured permeability ratio P_{TMA}/P_{Cl} is generally near 0.5. In a gallbladder with very low leakage conductance (e.g., uncorrected $P_{Na}/P_{Cl}\sim 15$), even the uncorrected value of P_{TMA}/P_{Na} is very low ($0.50/15=0.03$), and the value corrected by Eq. (3) is 0.0. However, if leakage conductance is high (e.g., uncorrected $P_{Na}/P_{Cl}\sim 2.0$), the uncorrected P_{TMA}/P_{Na} is now $0.50/2=0.25$, although the corrected value is still 0.

Our present experiments with nitrogenous cations provide two further types of evidence that chloride conductance is in a free-solution leakage pathway. As an illustration of the first type, consider the cation trimethylamine [$(CH_3)_3NH^+$], whose structure suggests that it should be relatively impermeant, for reasons to be discussed later. In a series of experiments in gallbladders of four species (frog, rabbit, guinea-pig, and *Necturus*), including some preparations with high leakage conductances (preparations that would have been rejected for purposes of the other experiments described in this paper), the uncorrected value of P_X/P_{Na} for $X=(CH_3)_3NH^+$ was sometimes as high as 0.25. However, in these experiments we noticed that P_X/P_{Na} (uncorrected) varied over a much wider range than did P_X/P_{Cl} (uncorrected), that variations in P_{Na}/P_{Cl} (uncorrected) and in P_X/P_{Cl} (uncorrected) were not correlated, but that variations in P_{Na}/P_{Cl} (uncorrected) and in P_X/P_{Na} (uncorrected) were closely correlated. The average value of P_X/P_{Cl} (uncorrected) was 0.48 ± 0.06, which is close to the free-solution mobility ratio of 0.51. In all four species studied the average value of P_X/P_{Cl} fell between 0.43 and 0.52, although the average value of P_K/P_{Cl} (uncorrected) ranged from 4 to 23 in these experiments. Thus, variations in P_X and in P_{Cl} were closely correlated and stood in the free-solution mobility ratio, while P_{Na} or P_K varied independently. After correction by Eq. (3), P_X/P_{Na} was indistinguishable from zero. Thus, essentially all permeability of $(CH_3)_3NH^+$ as well as of Cl^- is in the leakage pathway. Similarly, for other nitrogenous cations whose molecular structure suggests that permeability in the selective tight-junction channel should be near zero, the uncorrected ratio P_X/P_{Cl} is close to the free-solution mobility ratio, and the corrected P_X/P_{Na} value (Table 4) is near zero.

As a second illustration of the effect of the leakage pathway on nitrogenous cation permeability, Fig. 1 plots uncorrected and corrected values of P_X/P_{Na} against uncorrected values of P_{Na}/P_{Cl}, for $X=$dimethylamine ($(H_3C)_2NH_2^+$) in frog gallbladder (Fig. 1*a*) and for $X=$methylethylamine ($H_3C-NH_2^+-H_2C-CH_3$) in rabbit gallbladder (Fig. 1*b*). In both cases P_X/P_{Na} (uncorrected) decreases regularly with increasing P_{Na}/P_{Cl} (uncor-

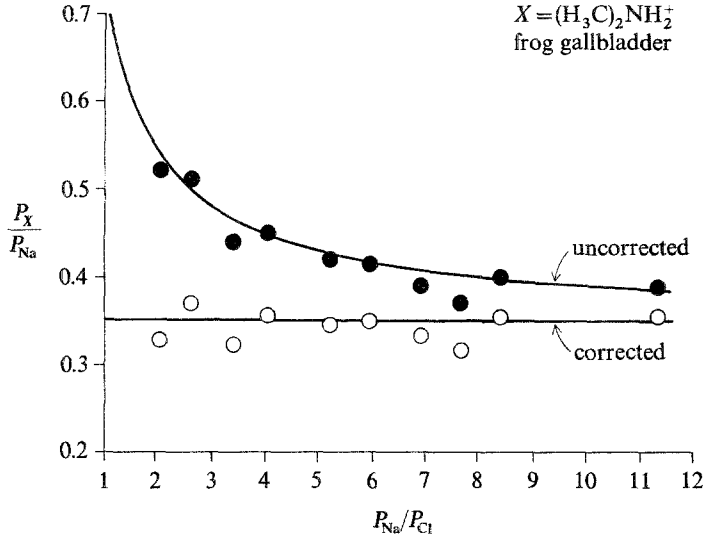

a

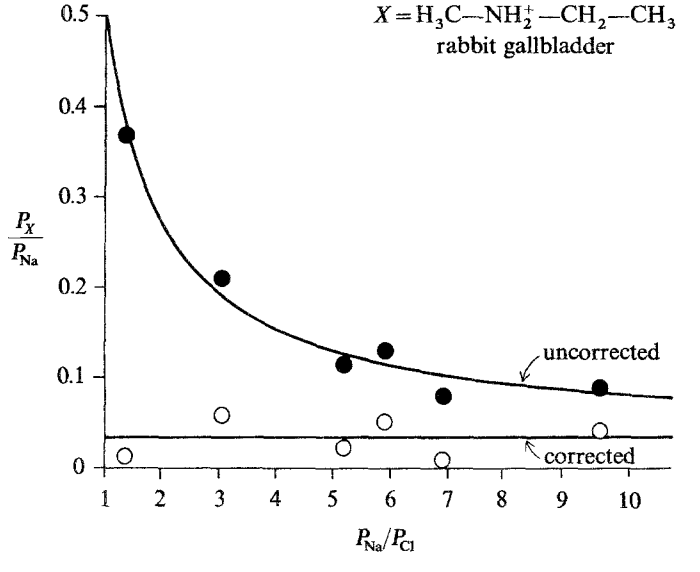

b

Fig. 1. Effect of the leakage pathway correction (Eq. (3)) on cation-to-cation permeability ratios P_X/P_{Na} in gallbladder. P_X/P_{Na} (ordinate) is plotted as a function of P_{Na}/P_{Cl} (abscissa) measured in the same gallbladder. (*a*) Based on the cation $X=(H_3C)_2NH_2^+$ in frog gallbladder; (*b*) $X=H_3C-NH_2^+-CH_2-CH_3$ in rabbit gallbladder. • uncorrected P_X/P_{Na} values calculated from Eq. (2); ○ the corresponding P_X/P_{Na} values corrected for leakage conductance by Eq. (3). P_{Na}/P_{Cl} values are uncorrected. The correction assumes that all chloride conductance of gallbladder is in a leakage pathway in which ionic conductance ratios equal free-solution mobility ratios. The horizontal line "corrected" is the average value of the points ○, while the curve "uncorrected" is the best fit of the points • to Eq. (3). Note that in both figures uncorrected P_X/P_{Na} values (•) vary markedly with P_{Na}/P_{Cl}, while corrected values (○) are independent of P_{Na}/P_{Cl}; and that Eq. (3) provides a good fit to the experimental points •. The conclusion is that apparent variation in P_X/P_{Na} is due entirely to variation in leakage conductance

rected), whereas P_X/P_{Na} (corrected) is independent of P_{Na}/P_{Cl} (uncorrected). The observed variation in P_X/P_{Na} (uncorrected) is well fitted by Eq. (3), as seen in the fit of the theoretical curve to the experimental points of Fig. 1. Thus, apparent variation in cation-to-cation permeability ratios among gallbladders with different P_{Cl}/P_{Na} values largely represents distortion of a constant P_X/P_{Na} value in native gallbladder by effects of a leakage pathway containing all G_{Cl}.

In the remainder of the present paper we drop the subscript m from $(P_X/P_Y)_m$ of Eq. (3) and use P_X/P_{Na} to mean permeability ratios corrected for the leakage pathway.

Results

Permeability Determinations are Uninfluenced by the Presence of the Neutral Form of the Cation

Most of the cations studied are in equilibrium with a neutral form and a dissociable proton, via a reaction of the type $YH^+ \rightleftarrows Y + H^+$. The presence of the neutral form could cause errors in measuring the permeability of the charged form. For example, if $P_Y \gg P_{YH^+}$, permeation of the form Y and equilibration of Y and YH^+ within unstirred layers adjacent to the membrane could reduce the effective concentration gradient of YH^+ immediately across the membrane, even though $(YH^+) \gg (Y)$ (LeBlanc, 1971). Furthermore, a dimer or polymer involving the protonated and neutral forms of the cation (e.g. $YH^+ Y$), or involving an anion and molecules of the protonated form (e.g., $YH^+ OH^- YH^+$ or $YH^+ Cl^- YH^+$), might contribute to measured permeability, since an ion whose charge is delocalized over a large volume or buried in a large dielectric cage might be significantly soluble in the hydrocarbon of the epithelial cell membranes. Such effects of the neutral form on measured permeabilities have been demonstrated or proposed for weak-acid uncouplers of oxidative phosphorylation (Liberman & Topaly, 1968; Finkelstein, 1970; LeBlanc, 1971).

In our experiments the solution pH was almost always at least two pH units below the pK_a of the cation studied, so that $(Y)/(YH^+) \leqq 0.01$. (The sole exceptions were with $HO-NH_3^+$ and $HO-NH_2^+-CH_3$, which have $pK_a \simeq 6.0$ and were studied at pH 5.0, so that $(Y)/(YH^+) = 0.1$; these two solutes were excluded from most of our analyses.) Five types of evidence rule out significant contributions of the neutral form to our measured permeabilities and show that it is the cationic form whose permeability is being measured:

1. Permeabilities of six cations were compared at pH 5.0 and 7.0, both in frog and in rabbit gallbladders. All six cations are ones with $pK_a \geqq 9.25$ (most of them ~ 10.7), so that $(YH)/(Y^+)$ varied over a 100-fold range, from ca. 2×10^{-4} to 2×10^{-6}, in these comparisons. The results of three experiments in each animal species are summarized in Table 1, which shows

Table 1. Comparison of permeability coefficients P_X/P_{Na} at pH 5.0 and pH 7.0

X	Frog		Rabbit	
	pH 7.0	pH 5.0	pH 7.0	pH 5.0
NH_4^+	1.73 ± 0.03	1.62 ± 0.05	1.42 ± 0.04	1.43 ± 0.05
$H_3C-NH_3^+$	0.80 ± 0.02	0.78 ± 0.02	0.46 ± 0.08	0.43 ± 0.02
$H_3C(CH_2)_2NH_3^+$	0.33 ± 0.03	0.34 ± 0.05	0.16 ± 0.05	0.17 ± 0.02
$H_3C(CH_2)_5NH_3^+$	0.29 ± 0.05	0.26 ± 0.05	0.41 ± 0.03	0.40 ± 0.02
$HOCH_3(CH_2)_5NH_3^+$	0.01 ± 0.03	0.01 ± 0.02	0.00 ± 0.03	0.00 ± 0.04

P_X/P_{Na} values as calculated from biionic potentials according to Eq. (3) are compared at pH 7.0 and pH 5.0, for the five cations listed in the first column. The P_X/P_{Na} values at pH 7.0 are reproduced from Table 3, while those at pH 5.0 are based on measurements in three gallbladders of each species. Note that P_X/P_{Na} is virtually independent of pH in this range. Errors in this and other tables are given as $\pm$SEM.

that P_{YH^+}/P_{Na^+} is independent of pH between 5.0 and 7.0 for these cations in both species. In addition to demonstrating that 100-fold variation in (Y) does not affect determinations of P_{YH^+}, this experiment also shows that P_{YH^+}/P_{Na^+} is independent of pH between pH 7.0 and 5.0, although cation-to-cation permeability ratios do change at lower pH values (Fig. 5; Moreno & Diamond, 1974*b*).

2. The permeability of methylamine ($H_3C-NH_3^+ \rightleftarrows H_3C-NH_2 + H^+$) was compared at pH 6.0 and pH 7.0 by means of ^{14}C tracer fluxes measured in standard Ringer's solution (*see* Moreno, 1975*b*, for details of the methods and permeability calculations). The component of the total measured permeability attributable to permeation through the leakage pathway was calculated from the chloride conductance and subtracted from the total measured permeability to yield a value corrected for permeation of $P_{H_3C-NH_3^+}$ through the leakage pathway. This correction procedure makes the same assumptions as does Eq. (3): that G_{Cl} is entirely in the leakage pathway, and that partial ionic conductance ratios in this pathway equal ratios of free-solution mobilities. Table 2 summarizes, for both frog and rabbit gallbladders, the corrected and uncorrected $P_{methylamine}$ values at pH 6.0 and 7.0. The table makes it obvious that in neither species does the shift from pH 7.0 to 6.0 affect $P_{methylamine}$, either before or after correction. Since the pK_a of methylamine is ca. 10.7, the concentration of the form H_3C-NH_2 decreases 10-fold from pH 7.0 to 6.0, while the relative change in the concentration of $H_3C-NH_3^+$ is negligible. Thus, Table 2 implies that the form $H_3C-NH_3^+$ accounts for virtually all of the tracer flux, and that the flux of H_3C-NH_2 is negligible.

Table 2. Comparison of $P_{methylamine}$ at pH 6.0 and 7.0

pH	$P_{methylamine}$ (cm/sec $\times 10^{-6}$)			
	Frog		Rabbit	
	uncorrected	corrected	uncorrected	corrected
7.0	8.1 ± 1.0	6.0 ± 0.6	19.9 ± 0.7	14.5 ± 0.8
6.0	8.0 ± 0.8	5.8 ± 0.8	20.3 ± 1.9	14.9 ± 2.0

The flux of ^{3}H-labeled methylamine ($H_3C-NH_3^+ \overset{H^+}{\rightleftarrows} H_3C-NH_2$) was measured in two gallbladders of each species at pH 7.0 and 6.0. "Uncorrected" values refer to measured values, from which calculated permeability in the shunt was subtracted as described in the text to obtain the "corrected" values. Note that in each species $P_{methylamine}$ is unaffected by this change in pH, implying that the form $H_3C-NH_3^+$ accounts for virtually the whole flux.

3. The permeability of methylamine may be calculated either from tracer fluxes (as in the preceding paragraph) or from electrical measurements (as in the remainder of this paper). Both in frog and in rabbit gallbladders, these two methods yield essentially the same permeability value (Moreno, 1975*b*). Thus, essentially all the tracer flux is due to the form $H_3C-NH_3^+$, as also shown by the experiment of the preceding paragraph. In addition, in each species the agent 2,4,6-triaminopyrimidinium reduces both the tracer and electrical permeability of methylamine by the same factor as it reduces P_{Na}, further indicating that both cations traverse gallbladder by the same tight-junctional route (Moreno, 1975*b*).

4. Stopping the stirring bars and increasing unstirred layer thickness causes no more decrease in YH^+/Na^+ biionic potentials than in alkali cation biionic potentials, whereas there should be a larger decrease if dissipation of the local (YH^+) gradient by permeating Y were significant.

5. Since permeation of solutes through lipid membranes decreases with increasing hydrogen-bonding ability of the solute (Collander, 1949, 1954; Diamond & Wright, 1969*a*, *b*), a significant component of permeation via membrane lipid would tend to cause measured P_{YH^+} values to be smaller for cations with increasing hydrogen-bonding ability. The reverse is true (Figs. 4, 10 and 11).

Thus, except perhaps in the case of the two cations with the lowest pK_a values, $HO-NH_3^+$ and $HO-NH_2^+-CH_3$ ($pK_a \simeq 6.0$), permeability determinations are uninfluenced by the very low concentrations of the neutral form of the cation present.

Table 3. Permeabilities of nitrogenous cations

No.	Name	Structure	$(MW)^{-1/3}$	u_X/u_{Na}	(P_X/P_{Na})		$(P_X/P_{Na})'$		S_X
					Frog	Rabbit	Frog	Rabbit	
1	ammonium	NH_4^+	18.04	1.55	1.73 ± 0.03 (16)	1.42 ± 0.04 (13)	2.48	3.23	0.58
2	methylamine	$H_3C-NH_3^+$	32.07	1.14	0.80 ± 0.02 (8)	0.46 ± 0.08 (3)	1.28	1.34	0.40
3	ethylamine	$H_3C-CH_2-NH_3^+$	46.09	0.828	0.50 ± 0.02 (6)	0.21 ± 0.03 (3)	0.93	0.89	0.30
4	*n*-propylamine	$H_3C(CH_2)_2NH_3^+$	60.12	0.716	0.33 ± 0.03 (8)	0.16 ± 0.05 (4)	0.60	0.64	0.34
5	allylamine	$H_2C=CH-CH_2-NH_3^+$	58.11	0.716	0.34 ± 0.03 (3)	0.11 ± 0.02 (3)	0.68	0.53	0.23
6	isopropylamine	$(H_3C)_2CH-NH_3^+$	60.12	0.635	0.27 ± 0.02 (3)	0.02 ± 0.02 (3)	0.75	0.23	0.06
7	*t*-butylamine	$(H_3C)_3C-NH_3^+$	74.14	0.612	0.11 ± 0.04 (3)	0.02 ± 0.08 (3)	0.34	0.36	0.13
8	azirane	$H_2C-CH_2-NH_2^+$ (ring)	44.08	1.02	0.40 ± 0.08 (3)	0.21 ± 0.06 (3)	0.76	1.00	0.38
9	dimethylamine	$(H_3C)_2NH_2^+$	46.09	0.944	0.35 ± 0.02 (6)	0.10 ± 0.03 (6)	0.96	1.04	0.19
10	methylethylamine	$H_3C-NH_2^+-CH_2-CH_3$	60.12	0.727	0.18 ± 0.02 (3)	0.03 ± 0.04 (3)	0.56	0.38	0.10
11	hydrazine	$H_2N-NH_3^+$	33.05	1.18	1.13 ± 0.02 (6)	1.05 ± 0.03 (6)	1.58	2.25	0.65
12	methylhydrazine	$H_3C-NH-NH_3^+$	47.08	0.949	0.51 ± 0.02 (3)	0.30 ± 0.05 (3)	0.92	1.17	0.41
13	formamidine	$H_2N-CH=NH_2^+$	45.06	1.01	1.31 ± 0.02 (6)	1.03 ± 0.06 (6)	2.32	3.89	0.55
14	acetamidine	$H_2N-(CH_3)C=NH_2^+$	59.09	0.667	0.55 ± 0.07 (3)	0.19 ± 0.02 (3)	1.13	1.05	0.25
15	guanidine	$(NH_2)_2C=NH_2^+$	60.08	1.00	0.94 ± 0.06 (6)	0.70 ± 0.02 (3)	1.64	2.57	0.52
16	aminoguanidine	$(NH_2)_2C=NH^+-NH_2$	75.09	1.20	0.89 ± 0.06 (3)	0.57 ± 0.04 (3)	1.55	2.05	0.45
17	methylguanidine	$(NH_2)_2C=NH^+-CH_3$	74.11	0.640	0.69 ± 0.04 (3)	0.26 ± 0.06 (3)	1.47	1.51	0.26
18	biguanidine	$NH=C(NH_2)-NH-C(NH_2)=NH_2^+$	103.13	0.541	0.23 ± 0.06 (4)	0.07 ± 0.04 (3)	0.55	0.55	0.21
19	triaminoguanidine	$(H_2N-NH)_2C=NH^+-NH_2$	105.12	0.636	0.55 ± 0.05 (3)	0.28 ± 0.03 (3)	1.24	1.99	0.37
20	ethylenediamine	$H_2N-CH_2-CH_2-NH_3^+$	61.11	0.723	0.32 ± 0.01 (3)	0.18 ± 0.02 (3)	0.60	0.77	0.32
21	aminoethanethiol	$HS-CH_2-CH_2-NH_3^+$	78.15	0.712	0.48 ± 0.06 (3)	0.21 ± 0.02 (3)	0.92	0.97	0.25
22	trimethylamine	$(H_3C)_3NH^+$	60.12	0.822	< 0.02 (3)	< 0.02 (3)	—	—	—
23	tetramethylammonium	$(H_3C)_4N^+$	74.14	0.732	< 0.02 (3)	< 0.02 (3)	—	—	—
24	6-amino-1-hexanol	$HO(CH_2)_6NH_3^+$	118.19	0.396	< 0.02 (3)	< 0.02 (3)	—	—	—
25	hydroxylamine	$HO-NH_3^+$	34.04	1.03	1.41 ± 0.03 (3)	1.63 ± 0.08 (3)			
26	methylhydroxylamine	$H_3C-NH_2^+-OH$	48.07	0.915	0.98 ± 0.01 (3)	0.74 ± 0.05 (3)			
27	ethanolamine	$HO-CH_2-CH_2-NH_3^+$	62.09	0.804	0.25 ± 0.01 (3)	0.07 ± 0.01 (3)			
28	methoxyethylamine	$H_3C-O-CH_2-CH_2-NH_3^+$	76.11	0.738	0.07 ± 0.06 (3)	0.08 ± 0.05 (3)			

29	1,3-aminopropanol	$HO-CH_2-CH_2-CH_2-NH_3^+$	76.11	0.667	0.08 ± 0.02 (3)	0.12 ± 0.02 (3)
30	1,2-aminopropanol	$H_3C-CH(OH)CH_2-NH_3^+$	76.11	0.640	0.09 ± 0.01 (3)	0.15 ± 0.04 (3)
31	2,1-aminobutanol	$H_3C-CH_2-CH_2(NH_3^+)CH_2OH$	89.14	0.501	0.03 ± 0.08 (3)	0.11 ± 0.04 (3)
32	2-amino-2-hydroxy-methyl-1,3-propanediol	$(HO-CH_3)_3CNH_3^+$	122.14	0.398	0.03 ± 0.04 (3)	0.13 ± 0.01 (3)
33	1-amino-5-pentanol	$HO(CH_2)_5NH_3^+$	104.13	0.393	0.121 (1)	0.06 ± 0.03 (3)
34	choline	$(H_3C)_3N^+-CH_2-CH_2OH$	122.07	0.393	0.07 ± 0.04 (3)	0.09 ± 0.05 (3)
35	imidazol	$HC=CH-NH-CH=NH^+$	69.08	0.882	0.32 ± 0.01 (3)	0.28 ± 0.03 (3)
36	*n*-butylamine	$H_3C(CH_2)_3NH_3^+$	74.14	0.581	0.35 ± 0.03 (3)	0.17 ± 0.06 (4)
37	isobutylamine	$(H_3C)_2CH_2-CH_2-NH_3^+$	74.14	0.580	0.16 ± 0.03 (3)	0.18 ± 0.03 (3)
38	sec-butylamine	$H_3C-CH_2-CH(CH_3)NH_3^+$	74.14	0.557	0.16 ± 0.01 (3)	0.17 ± 0.03 (3)
39	diethylamine	$(H_3C-CH_2)_2NH_3^+$	74.14	0.537	0.28 ± 0.03 (3)	0.06 ± 0.03 (3)
40	*n*-pentylamine	$H_3C(CH_2)_4NH_3^+$	88.17	0.503	0.32 ± 0.03 (17)	0.26 ± 0.08 (5)
41	isopentylamine	$(H_3C)_2CH_2-CH_2-CH_2-NH_3^+$	88.17	0.514	0.27 ± 0.03 (3)	0.17 ± 0.05 (3)
42	*n*-hexylamine	$H_3C(CH_2)_5NH_3^+$	102.19	0.440	0.29 ± 0.05 (8)	0.41 ± 0.03 (11)
43	dipropylamine	$(H_3C-CH_2-CH_2)_2NH_2^+$	102.19	0.351	—	0.12 ± 0.04 (3)
44	triethylamine	$(H_3C-CH_2)_3NH^+$	102.19	0.449	0.03 (1)	0.06 (1)
45	cyclohexylamine	$(C_2C)_5CH-NH_3^+$	100.19	0.466	0.29 ± 0.03 (3)	0.31 ± 0.08 (5)
46	*n*-heptylamine	$H_3C(CH_2)_6NH_3^+$	116.22	0.480	—	0.58 (1)
47	benzylamine	$C_6H_5-CH_2-NH_3^+$	108.16	0.429	0.46 ± 0.04 (10)	—
48	dibutylamine	$(H_3C-CH_2-CH_2-CH_2)_2NH_2^+$	130.25	0.329	0.24 ± 0.06 (2)	0.46 ± 0.04 (4)
49	diisobutylamine	$((H_3C)_2CH-CH_2)_2NH_2^+$	130.25	0.349	0.16 (1)	0.41 ± 0.04 (3)
50	tetraethylammonium	$(H_3C-CH_2)_4N^+$	130.25	0.431	0.06 ± 0.05 (4)	0.07 ± 0.02 (3)
51	tripropylamine	$(H_3C-CH_2-CH_2)_3NH^+$	144.27	0.385	0.15 ± 0.03 (10)	0.29 ± 0.05 (3)
52	tributylamine	$(H_3C-CH_2-CH_2-CH_2)_3NH^+$	186.36	0.278	0.22 (1)	0.45 ± 0.04 (10)

Each cation named in column 2 is assigned a number in column 1, used for coding experimental points in the figures. Column 3 gives the structure; column 4, the molecular weight; column 5, the free-solution mobility ratio u_X/u_{Na} at 150 mM, measured by us as discussed in the Appendix (except that values for *n*-heptylamine and *n*-pentylamine are from Desnoyers *et al.* (1969), the value for allylamine is assumed equal to that of *n*-propylamine, and the value for methylethylamine was interpolated by averaging the equivalent conductances of dimethylamine and diethylamine); columns 6 and 7, the "raw" permeability coefficients in frog and rabbit gallbladders ("raw" = not corrected for steric restriction in the permeation channel); columns 8 and 9, the permeability coefficient corrected for steric restriction, as discussed on pp. 227–228; and column 10, the steric factor $S_X \equiv (P_X/P_{Li})_{rabbit}/(P_X/P_{Li})_{frog}$, as discussed on p. 220.

Analysis of "Raw" Permeability Coefficients

Table 3 summarizes, for all cations tested, the molecular weight MW, the free-solution mobility ratio u_X/u_{Na}, the "raw" permeability ratio P_X/P_{Na} in frog and rabbit gallbladders as calculated from Eq. (3), the permeability ratio $(P_X/P_{Na})'$, in each species corrected for steric restriction in the permeation channels as discussed on pp. 227–228, and the "steric factor" S_X as discussed on pp. 220–221.

In our further analysis from this page until p. 231, we consider only the first 24 cations in Table 3. All available evidence is consistent with the assumption that these cations permeate predominantly via tight junctions. The remaining 28 cations fall into two groups: 1. Cations no. 25–34, which contain an oxygen atom and have a measurable permeability, are discussed separately on pp. 231–233 and are suspected in rabbit but not frog gallbladder of having a permeability component via polar pathways in cell membranes. 2. Cations no. 35–52 share the properties of significant lipid solubility, a long hydrocarbon chain, few hydrogen-bonding groups besides the amino group, and a measurable permeability. These cations are suspected of having a permeability component via membrane lipid, and are discussed separately on pp. 233–239.

Figs. 2–4 depict some patterns of the "raw" P_X/P_{Na} values of cations no. 1–24 of Table 4:

Fig. 2 shows that P_X/P_{Na} in rabbit gallbladder increases with P_X/P_{Na} in frog gallbladder. The two sets of values are closely correlated, though the values for all 24 nitrogenous cations analyzed lie below the line of identity.

Figs. 3*a* and 3*b* plot P_X/P_{Na} against $\sqrt[3]{(MW)}$ in frog and rabbit gallbladders, respectively. The first impression both figures give is that the experimental points scatter widely. On closer inspection, much of the scatter appears related to differences among cations in the number of protons available for forming hydrogen bonds (abbreviated n_H). It will be recalled that H covalently bonded to electronegative atoms, notably N, O and F, interacts with adjacent electronegative atoms on another or the same molecule, the interaction strength being weaker than the energy of a covalent bond but greater than the energy of van der Waals forces alone. The attractive forces in this interaction, besides van der Waals forces, are the energy of electron delocalization (resonance forces), and the electrostatic forces between the partial negative charges on the electronegative atoms and the partial positive charge on H (Hadzi, 1959; Pimentel & McClellan, 1960). In Fig. 3 we use different symbols for the cations, depending on

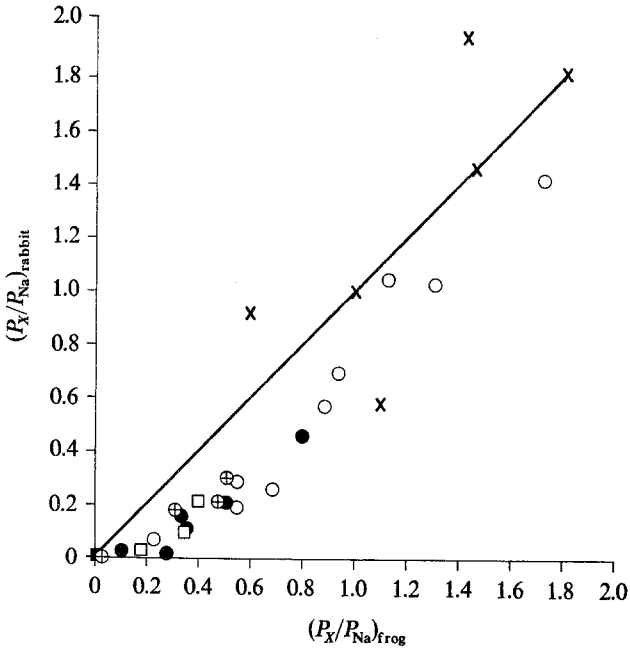

Fig. 2. "Raw" P_X/P_{Na} values for 24 nitrogenous cations and six monatomic cations in rabbit gallbladder (ordinate), plotted against values for the same cations in frog gallbladder (abscissa). Values are taken from columns 6 and 7 of Table 3. Symbols: ○ nitrogenous cations that can donate ≧4 protons for H-bond formation; ● nitrogenous cations with 3 donor protons; ⊕ nitrogenous cations that nominally have 4 donor protons but that behave as if they have 3, possibly due to intramolecular H-bonding; □ nitrogenous cations that can donate 2 protons; ■ nitrogenous cations that can donate 1 or 0 protons; × the metallic cations Cs^+, Rb^+, K^+, Na^+, Li^+, and Tl^+ (P_X/P_{Na} values from Moreno & Diamond, 1974*b*). The line is the line of identity. Note that rabbit and frog P_X/P_{Na} values for nitrogenous cations are closely correlated but that all lie below the line of identity

whether they possess four or more (○), three (●), effectively three (⊕), two (□), or one or zero (■) protons that can be donated to a suitable proton acceptor (e.g., an O or N on membrane functional groups such as $-COO^-$, projecting into a permeation channel across a tight junction). Fig. 3 shows that if one compares cations with the same molecular weight, permeability tends to increase with the number of donor protons n_H (for example, compare the ordinate values of the points ○, ●, □ and ■ around $\sqrt[3]{(MW)} = 3.9$ in Fig. 3*a* for frog gallbladder). Thus, $(H_2N)_2C=NH_2^+$, $(H_3C)_2CH-NH_3^+$, and $(H_3C)_2NH^+-CH_3$ have approximately the same size and shape, but the respective P_X/P_{Na} values in frog gallbladder are 0.94, 0.27, and <0.02, in the sequence of number of donor protons (6, 3 and 1, respectively). If one compares cations with the same number of donor protons, permeability increases with decreasing MW, as is best seen from the points

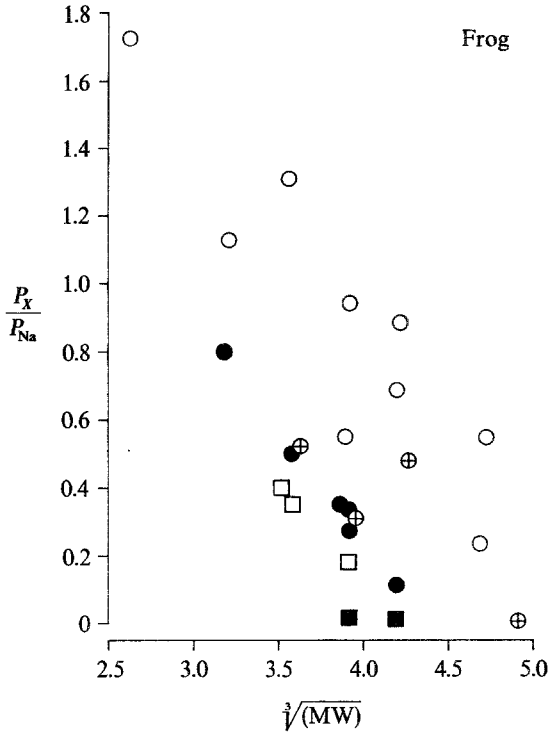

Fig. 3a

Fig. 3. The dependence of P_X/P_{Na} (ordinate) on cube root of molecular weight (abscissa). (*a*) Frog gallbladder; (*b*) rabbit gallbladder. Symbols refer to number of donor protons n_H on each cation (○ = ≧4, ● = 3, ⊕ ~ 3, □ = 2, ■ = 0 or 1), as explained in the legend of Fig. 2. Note that values scatter widely in each species, but that P_X/P_{Na} tends to increase with n_H at constant $\sqrt[3]{MW}$ (*see also* Fig. 4), and tends to decrease with $\sqrt[3]{MW}$ at constant n_H

○ or ● in frog or rabbit and points □ in frog. (MW dependence of P is not detectable for points ■ in both species and is barely detectable for points □ in rabbit, because these cations with few donor protons have low or undetectably low P_X/P_{Na} values.) The four cations represented by points ⊕ ($H_2N-CH_2-CH_2-NH_3^+$, $HO-(CH_2)_6-NH_2^+$, $HS-CH_2-CH_2-NH_3^+$, $H_3C-NH-NH_3^+$) possess four or five donor protons but have P_X/P_{Na} values below those of other cations with four or more donor protons, and similar to cations with three donor protons. At least the first two of these aberrant cations could form intramolecular H-bonds

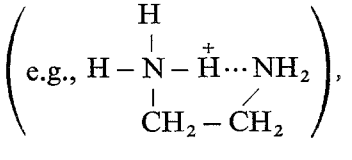

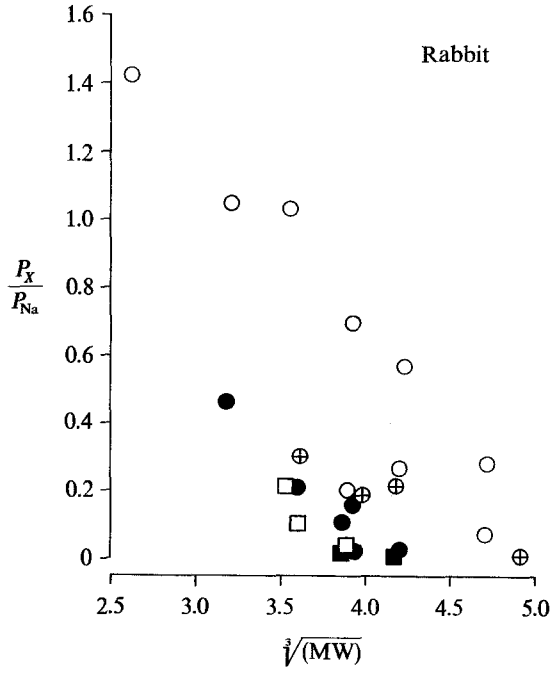

Fig. 3b

so that the number of protons available for H-bonding with membrane proton acceptors might be less than four (*see also* Fig. 14*a* and p. 232).

Since free-solution mobilities u_X/u_{Na} tend to decrease with increasing MW, one might wonder whether the decrease in P_X/P_{Na} with $\sqrt[3]{MW}$ displayed by Fig. 3 is because P equals the product of a factor proportional to number of donor protons (e.g., a binding energy between the cation and membrane proton acceptors) times a factor proportional to free-solution mobilities (e.g., mobility or frictional forces within the membrane channel). To test this possibility, Figs. 4*a* and 4*b* plot $(P_X/P_{Na})/(u_X/u_{Na})$ for frog and rabbit gallbladders, respectively, against n_H. Fig. 4 makes the increase in permeability with number of donor protons more obvious than does Fig. 3. However, the MW dependence of permeability is not eliminated by dividing P_X by u_X: for a given number of donor protons, $(P_X/P_{Na})/(u_X/u_{Na})$ is lower for solutes with higher MW. Evidently, the inverse size dependence is steeper for permeation through gallbladder than for diffusion in free solution.

This preliminary analysis of the "raw" experimental data shows that permeability of nitrogenous cations through the selective channels of gallbladder tight junction depends both on H-bonds and on molecular size.

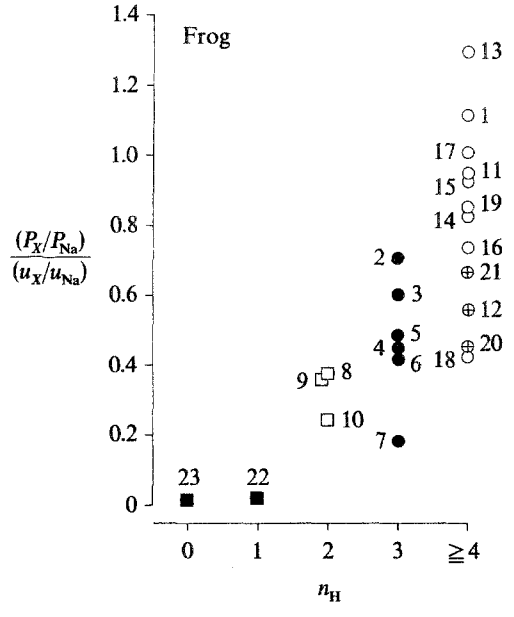

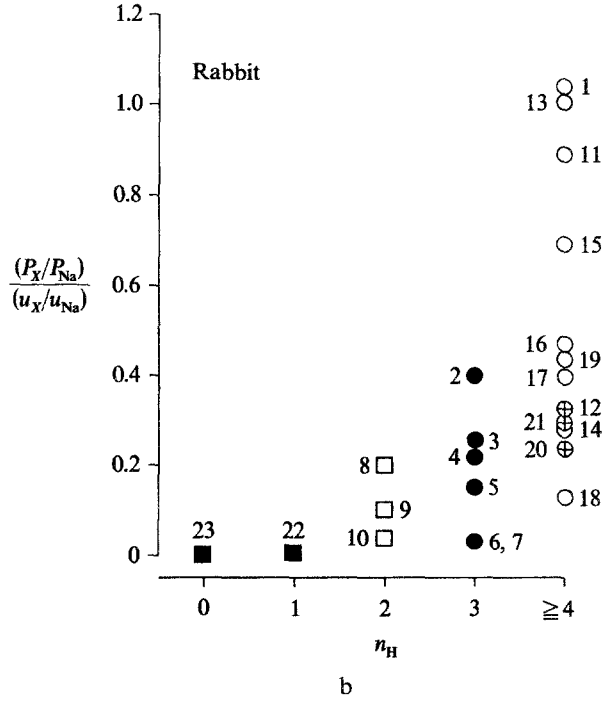

Fig. 4. Dependence of $(P_X/P_{Na})/(u_X/u_{Na})$ for nitrogenous cations, the permeability ratio divided by the free-solution mobility ratio, on the cation's number of donor protons n_H. Symbols as in Figs. 2 and 3. Numbers identify cations as coded in column 1 of Table 3. (*a*) Frog gallbladder; (*b*) rabbit gallbladder. $(P_X/P_{Na})/(u_X/u_{Na})$ tends to increase with n_H

However, the analysis has not succeeded in completely separating these two dependences or in treating them quantitatively. In the next section we present evidence suggesting that permeability also depends on still another factor, namely, electrostatic field strength.[2]

Selectivity Isotherms for Nitrogenous Cations

In studying discrimination of permeating alkali cations by gallbladder, we found that gallbladders from different individual animals of the same species showed systematically related differences in relative permeability coefficients of different cations (Moreno & Diamond, 1973*b*, 1974*b*). That is, if the P_X/P_K value for some cation X^+ was plotted against P_{Na}/P_K measured in the same animal, and such measurements were made in many animals, the points did not scatter at random but clustered around a curve, the so-called empirical selectivity isotherm for that cation. When P_X/P_K and P_{Na}/P_K values were shifted in the same animal by lowering bathing pH to 4.1 or below, the points shifted along the same isotherms as those defined by individual variation. The isotherms, and the permeability sequences they defined, were consistent with Eisenman's (1961, 1962, 1965*b*) theoretical calculations of alkali cation selectivity sequences, based on electrostatic field strength of cation-binding sites in the membrane as the controlling variable.[3]

Our previous study included one nitrogenous cation, NH_4^+, whose permeability coefficient P_{NH_4}/P_K was found to vary among individual animals and with pH and to define as neat a selectivity isotherm (when plotted against P_{Na}/P_K) as did P_X/P_K determinations for the alkali cations. We have therefore attempted to construct similar selectivity isotherms for

2 As discussed on p. 210 and p. 220, electrostatic forces between H-bonded atoms with partial charges constitute one of the three principal attractive energies of an H-bond. In addition to contributing to H-bond strength, electrostatic forces may also contribute significantly to solute-membrane interactions not involving H-bonds. Thus, H-bonds and electrostatic field strength are partly but not completely distinct as determinants of nitrogenous cation permeability.

3 If the electrostatic fields of membrane sites and of water exhibit different radial dependence, electrostatic considerations predict alkali cation selectivity sequences that are related to ionic size (Eisenman, 1962; *see* Krasne & Eisenman, 1973, for more detailed discussion). Similar size-related sequences are also predicted from considerations of deformation energies. Thus, it may be difficult to decide whether selective effects of alkali cations that are observed to be size-related originate in electrostatic forces or in deformation forces. However, as discussed in footnote 4 on p. 220, for nitrogenous cations the results depicted in Fig. 6 agree with the interpretation that variation in the abscissa values of isotherms such as Fig. 5 or 6 represents primarily variation in electrostatic forces rather than in deformation energies.

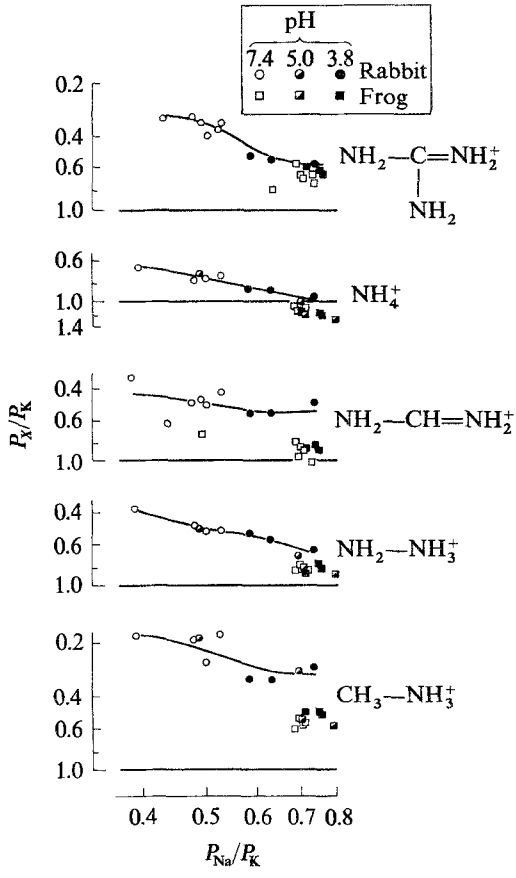

Fig. 5. So-called selectivity isotherms for five nitrogenous cations in gallbladder. The abscissa gives P_{Na}/P_K values measured in the gallbladders of each of 12 individual frogs or 12 individual rabbits, at pH 7.4, 5.0, or 3.8 (*see* figure for symbols). The ordinate gives P_X/P_K measured in the same individual gallbladder at the same pH, where X is in each case the nitrogenous cation indicated on the right of each graph. The scales are logarithmic, and the ordinate is inverted. Thus, sets of points located along the same imaginary vertical line represent P_X/P_K values for several different cations measured in the same animal at the same pH. The solid curves are the second-order polynomials fitted through the points for each cation in rabbit, and are called selectivity isotherms. That the points do define empirical isotherms instead of scattering at random means that P_X/P_K and P_{Na}/P_K are closely correlated (e.g., because both are responding to the same physical variable). The horizontal line at $P_X/P_K = 1.0$ is the K^+ isotherm in each case. In frog the range of experimental points is too narrow to permit calculation of isotherms

four other nitrogenous cations (guanidine, formamidine, hydrazine and methylamine), as depicted in Fig. 5. The method was to measure P_X/P_K values for several of these cations, Na^+, and NH_4^+ in gallbladders from 12

individual rabbits and 12 individual frogs, first at pH 7.4, then at either pH 5.0 or 3.8 or both, and finally at pH 7.4 again. Fig. 5 plots P_X/P_K for each nitrogenous cation against P_{Na}/P_K measured in the same gallbladder at the same pH. Four conclusions follow from Fig. 5:

1. For all five nitrogenous cations studied, P_X/P_K is higher at pH 3.8 than at pH 7.4 in every individual rabbit studied (compare ordinate values of points • and ○).

2. Among individual rabbits studied at pH 7.4, P_X/P_K clearly increases with increasing P_{Na}/P_K for $X = H_2N-NH_3^+$ and NH_4^+. For these two cations it is apparent that the shift in P_X/P_K on proceeding from pH 7.4 to pH 3.8 is in the same direction as the shift in proceeding at pH 7.4 from an individual gallbladder with low P_{Na}/P_K to one with high P_{Na}/P_K. In the cases of the other three cations there is too much scatter or too few rabbits to determine whether individual variation in P_X/P_K and in P_{Na}/P_K is correlated.

3. For this particular group of frogs, there is too little individual variation or pH variation in either P_{Na}/P_K or P_X/P_K to determine whether variations in two cations are correlated. Comparison of the P_{Na}/P_K and P_{NH_4}/P_K ranges of our Fig. 5 with those of Fig. 1 of Moreno and Diamond (1974*b*) emphasizes that the frogs of Fig. 5 were too homogenous or too few to permit conclusions.

4. It is nevertheless clear that, for a given P_{Na}/P_K value, P_X/P_K is conspicuously lower in rabbit than in frog for $H_3C-NH_3^+$ and $H_2N-CH=NH_2^+$, and is somewhat lower in rabbit than in frog for NH_4^+, $(H_2N)_2C=NH_2^+$, and $H_2N-NH_3^+$.

Our previous studies of alkali cation selectivity were consistent with the interpretation that individual or pH-dependent variation in P_{Na}/P_K arises from variation in the electrostatic field strength of cation binding sites in membrane channels (Moreno & Diamond, 1973*b*, 1974*b*). These sites presumably consist of acidic groups in the negatively charged form, such as $-COO^-$ or $-HPO_4^-$. Reduction in the partial negative charge on the sites, due either to low pH or else to inductive effects of neighboring groups or else to lower-than-average site coordination number in a particular gallbladder, results in a shift of P_{Na}/P_K from left to right along the isotherms of Fig. 5, for reasons discussed by Eisenman (1961, 1962, 1965*b*; *cf. also* review by Diamond & Wright, 1969*a*, and discussion by Moreno & Diamond, 1974*b*, 1975). Thus, Fig. 5 suggests that variation in field strength of rabbit gallbladder sites does produce variation in P_X/P_K for nitrogenous

cations, as for alkali cations. The experiments in frog gallbladder were inadequate to test this question.

The differences in the P_X/P_K value of a given metallic cation between rabbit and frog gallbladders, at the same value of P_{Na}/P_K, were consistent with the interpretation that gallbladders of these two species differ in the steric restriction offered to permeating cations (Moreno & Diamond, 1973*b*, 1974*b*). For increasingly large metallic cations, P_X/P_K in rabbit lagged increasingly behind P_X/P_K in frog for a given P_{Na}/P_K value, suggesting that the permeation channel in rabbit is narrower than in frog. All five nitrogenous cations whose P_X/P_K values are depicted in Fig. 5 are larger than K^+. Since P_X/P_K values of all five cations are lower in rabbit than in frog at a given P_{Na}/P_K value, these species differences may be due to a narrower permeation channel in rabbit, as also concluded from the behavior of alkali cations. This hypothesis will be tested quantitatively on the following pages.

Estimation of Differences in Steric Restriction between Rabbit and Frog Gallbladders

If one just compares average P_X/P_K values in rabbit and frog gallbladders without taking account of the species difference in average P_{Na}/P_K values, the species difference in P_X/P_K may reflect differences in field strength as well as in steric restriction. Ideally, to isolate the steric contribution, one should proceed as for the alkali cations (Figs. 7 and 8 of Moreno & Diamond, 1974*b*) or as depicted in Fig. 5 for five nitrogenous cations. That is, for each cation one should construct the selectivity isotherms in rabbit and frog gallbladders by plotting P_X/P_K values *vs.* P_{Na}/P_K values; then read off the P_X/P_K value from the isotherm for each species at the same value of P_{Na}/P_K, to eliminate the contribution of species differences in field strength to species differences in P_X/P_K; and, finally, examine whether species differences in P_X/P_K as a function of cation radius are in accord with some theory based on steric restrictions. In practice, we would have enough experimental information to follow this procedure only for the five cations depicted in Fig. 5; we have not made enough experimental measurements to construct isotherms for other nitrogenous cations. However, the fact that isotherms for different nitrogenous cations in a given species are roughly parallel to each other and to the NH_4^+ isotherm suggests an alternative procedure to eliminate effects of interspecific differences in field strength. This fact is illustrated more clearly by Fig. 6, which plots each value of P_X/P_{NH_4} as a function of the P_K/P_{NH_4} value measured in the same individual animal at the

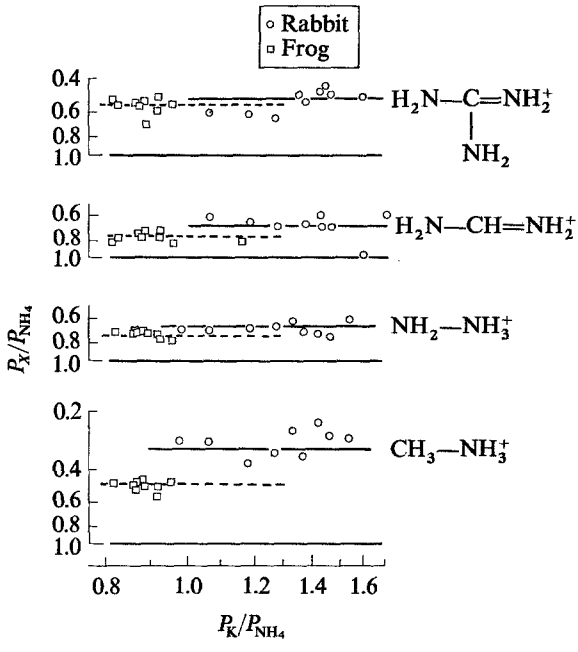

Fig. 6. Isotherms for four nitrogenous cations in rabbit (○) and frog (□) gallbladders, constructed in the same manner as Fig. 5, but referred to NH_4^+ rather than to K^+. P_X/P_{NH_4} in a given animal at a given pH is plotted against P_K/P_{NH_4} in the same animal at the same pH. Points for $X=NH_4^+$ are omitted; they lie along the horizontal line at $P_X/P_{NH_4}=1.0$ drawn below the points for each cation. The isotherms for each cation (solid line, rabbit; dashed line, frog) are horizontal lines drawn at the average value of P_X/P_{NH_4} in each animal. The fact that experimental points for each ion in each animal do define approximately horizontal lines means that P_X/P_{NH_4} is relatively insensitive to the variation in field strength thought to underlie variation in P_K/P_{NH_4}

same pH. For each cation in each species, an approximately horizontal line is obtained (because the isotherms of Fig. 5 are approximately parallel). For each cation, the rabbit line (solid line) lies above the frog line (dashed line), meaning lower permeability (interpreted as greater steric restriction, for reasons discussed in the next section) in the rabbit. If variation in P_K/P_{NH_4} can be interpreted as due to variation in field strength, then the P_X/P_{NH_4} values corresponding to the horizontal lines of Fig. 6 are approximately independent of field strength, since P_X/P_{NH_4} is independent of P_K/P_{NH_4}. Thus, for each cation X the ratio $S'_X \equiv (P_X/P_{NH_4})_{rabbit}/(P_X/P_{NH_4})_{frog}$ from Fig. 6 may depend mainly on steric factors and may be approximately independent of field strength, even though individual P_X/P_K values are not.[4]

4 Fig. 6 permits reassessment of the problem raised in the previous section, namely, how to distinguish effects of electrostatic field strength (e.g., Eisenman, 1961, 1962) from effects of deformation energies (e.g., Simon & Morf, 1973) on selectivity. If the

What is the Effective Molecular Radius of Permeating Cations?

If the ratio S'_X mainly means that the permeation channel is narrower in rabbit than in frog gallbladder, S'_X should decrease with increasing size of the permeating cation. To test this hypothesis, we calculated S'_X for each cation, as the ratio of the average P_X/P_K value divided by the average P_{NH_4}/P_K value in rabbit, divided by the corresponding ratio in frog. Multiplication of S'_X by the average value of $(P_{NH_4}/P_{Li})_{rabbit}/(P_{NH_4}/P_{Li})_{frog}$ ($=0.578$, from Moreno & Diamond, 1974*b*) then yields the factor $S_X \equiv (P_X/P_{Li})_{rabbit}/(P_X/P_{Li})_{frog}$, tabulated for each analyzed cation in Table 4.

For metallic cations, S_X calculated in this way decreases monotonically with ionic radius (Moreno & Diamond, 1974*b*, Fig. 8; this figure depicts $1/S_X$, which is called F_X). The Renkin equation (Renkin, 1954) describes steric restriction to permeation in rigid, right-circular-cylindrical pores:

$$Y_X \equiv (A_X/A) = [1-(r_X/R)^2][1-2.104(r_X/R)+2.09(r_X/R)^3-0.95(r_X/R)^5] \quad (4)$$

where r_X is the radius of the permeating solute species X, R the radius of the pore, A the cross-sectional area of the pore ($=\pi R^2$), and A_X the effective

---

physical variable corresponding to the abscissa of Fig. 5 or 6 is one that determines deformation energies (e.g., a pore radius or elasticity), permeabilities of cations of different size should change with this variable at different rates, and the isotherms of Fig. 5 or 6 should not be parallel but should have intersections. The same prediction follows (and is fulfilled for the alkali cations: Moreno & Diamond, 1974*b*, Figs. 11 and 12) if the variable corresponding to the abscissa of Fig. 5 or 6 is field strength of membrane sites and if the permeating cations can be well represented (as can the alkali cations) by spheres of differing radius with a point charge at the center. Thus, for the alkali cations a clear decision between electrostatic considerations and deformation energies as the more important factor in selectivity is difficult, because both yield prediction of the same selectivity sequences. This need not be the case, however, for nitrogenous cations. Suppose that ion-site attraction energies are dominated by hydrogen bonds, so that the cations are not adequately represented as a sphere with central point charge. If the abscissa of Fig. 5 or 6 still corresponds to variation in site field strength, so that the electrostatic component of the hydrogen bond varies along the abscissa, then the simplest expectation is for cations with different numbers or strengths of hydrogen bonds to yield parallel isotherms of non-zero slope in Fig. 5 (where P_X is taken relative to P of an alkali cation) and to yield parallel horizontal isotherms in Fig. 6 (where P_X is taken relative to P of another H-bonding cation, NH_4^+)—in contrast to the prediction based on deformation energies. The isotherms of Figs. 5 and 6 are in fact parallel and nonintersecting. They thus agree with the interpretation that site field strengths rather than deformation energies are what varies along the abscissa of Figs. 5 and 6. It is consistent with this interpretation that pH effects on the abscissa and on permeabilities of alkali cations are readily interpreted in terms of electrostatic forces (Moreno & Diamond, 1974*b*, pp. 302–303) but cannot be easily predicted from considerations of deformation energies.

area available for permeation of the solute. $Y_X = (A_X/A)$ is the factor by which the solute's permeability coefficient is reduced, compared to the value that would exist in the absence of any steric restriction. If one calculates by least-mean-squares the values of the equivalent pore radii R_{rabbit} and R_{frog} that yield the best fit of the Renkin factor

$$(Y_X/Y_{\text{Li}})_{\text{rabbit}}/(Y_X/Y_{\text{Li}})_{\text{frog}} \equiv S_X \tag{5}$$

to the experimental values of S_X for metallic cations, we showed previously that one obtains a good fit to the observed dependence of S_X on molecular size r_X (taken as the Ladd ionic radius, Ladd, 1968), with the equivalent pore radii estimated as $R_{\text{rabbit}} = 3.8$ Å, $R_{\text{frog}} = 5.9$ Å (Moreno & Diamond, 1974*b*, Fig. 8, pp. 296–299). The crucial problem in extending this analysis to nitrogenous cations is to obtain appropriate values of their molecular radii r_X. The remainder of this section is devoted to this problem.

The results of a simplistic attempt to solve this problem are depicted in Fig. 7. We calculated an effective van der Waals radius for each cation from CPK (Corey-Pauling-Koltum) molecular models, in which each atom has its covalent van der Waals radius. The sides *a*, *b* and *c* of the smallest rectangular box that could contain the cation were measured (tabulated as "van der Waals" measurements in Table 5), and the molecular radius was taken as $r_{vdw} \equiv (a+b+c)/6$ or half the average side length. In Fig. 7 the experimental S_X values of nitrogenous cations are plotted as a function of these r_{vdw} values, along with S_X values for metallic cations and the best-fit Renkin curve $(Y_X/Y_{\text{Li}})_{\text{rabbit}}/(Y_X/Y_{\text{Li}})_{\text{frog}}$ through the experimental points. There is much scatter in Fig. 7, but the scatter describes a pattern: the nitrogenous cations with $\geqq 4$ donor protons (points ○) almost all lie to the right of the Renkin curve while all those with two protons (□) and most of those with three protons (●) fall to the left of the curve. (Those with $\leqq 1$ proton are too impermeant to use in this analysis, since their P_X/P_{Na} values were too low to measure accurately.) That is, the selective ion channels of gallbladder tight junction see proton-rich cations as smaller than their van der Waals radii, or proton-poor cations as larger than their van der Waals radii. A further illustration of this pattern is that the separation between frog and rabbit isotherms (Fig. 6) is much larger for $H_3C-NH_3^+$ than for $H_2N-NH_3^+$, even though these two cations have nearly the same van der Waals radius and free-solution mobility. Evidently, the proton-rich $H_2N-NH_3^+$ behaves as if it were smaller than the proton-poor $H_3C-NH_3^+$ in gallbladder tight junction.

These systematic deviations in Fig. 7 suggest that proton-rich cations form H-bonds with oxygen proton-acceptors in the wall of the permeation

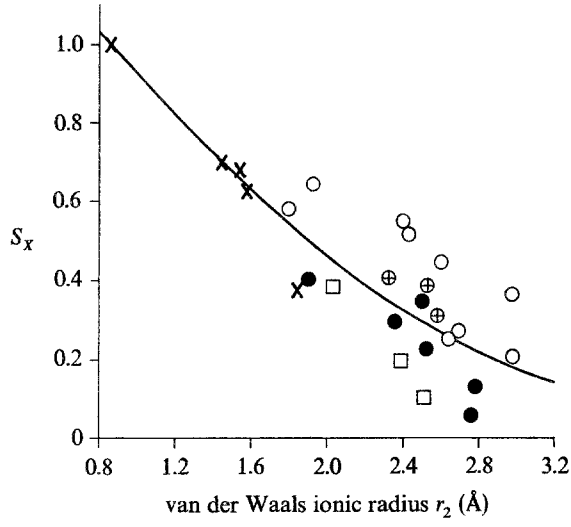

Fig. 7. The steric factor $S_X(\equiv(P_X/P_{Li})_{rabbit}/(P_X/P_{Li})_{frog}$; ordinate) as a function of molecular radius (abscissa), for 26 cations. As discussed in the text, S_X has the approximate significance of the relative permeability coefficient in rabbit divided by the relative permeability coefficient in frog, corrected for species differences in field strength of membrane cation-selective sites. For the nitrogenous cations the radius is taken as the van der Waals radius r_2 (*see* p. 223 for definition of r_2), calculated as $(a+b+c)/6$ from the dimensions in columns 2–4 of Table 5. For metallic cations (points X) the Ladd ionic radius is used. Cations are identified by symbols as in Fig. 2. The curve is the least-mean-squares fit of the Renkin factor $(Y_X/Y_{Li})_{rabbit}/(Y_X/Y_{Li})_{frog}$, from Eqs. (4) and (5), to the experimental S_X values and to the above choices of ionic radii. The resulting estimated equivalent pore radii are 5.1 and 8.0 Å in rabbit and frog gallbladders, respectively. Note that S_X decreases with molecular radius and that all values of S_X are $\leqq 1$, suggesting that S_X is mainly due to greater steric restrictions on larger cations in the narrower pores of rabbit gallbladder. Note also that there is much scatter, but that points ○ ($n_H \geqq 4$) lie to the right and points □ ($n_H = 2$) to the left of the mean curve. Thus, much of the scatter in this graph is because van der Waals radii fail to take account of an effective decrease in cation radius with increasing proton-donor ability

channel (i.e., the $-X-N-H\cdots O-$ interatomic distance is shorter than would be the case if the interaction between the proton and oxygen only involved van der Waals forces). Thus, in a hydrogen-bonding environment hydrogen-bonding solutes appear smaller than nonhydrogen-bonding solutes. Hille (1971, 1973, 1975) emphasized the importance of this fact for understanding nitrogenous cation selectivity by nerve's sodium channel. An extreme way to correct for this fact in calculating molecular radii would be to pretend that donor protons do not contribute to molecular size at all. We therefore recalculated a van der Waals radius r_{-H} for each cation from

CPK models from which all H atoms attached to N or O atoms had been removed. A plot of experimental S_X values against these r_{-H} values shows less scatter, and is better fitted by the Renkin curve Eq. (5), than Fig. 7.

It is unrealistic to pretend that donor protons do not contribute to molecular size at all. However, the pattern of the scatter in Fig. 7, and the improved fit of an $S_X - vs. - r_{-H}$ plot over Fig. 7, show that a realistic analysis of the steric effect should recognize that molecules with donor protons behave as if they are smaller than their van der Waals radii in the hydrogen-bonding environment of the permeation channel. This pattern provides a second, independent line of evidence (in addition to the evidence of Fig. 4) that the channel walls contain proton-acceptor H-bonding sites. We therefore compared alternative choices of molecular radii as follows:

1. The N-to-Y center-to-center interatomic distance (i.e., the hydrogen-bond length) in groups of the form $-N-H\cdots Y-$, where Y is either O,Cl, Br, or I, was tabulated from published crystallographic measurements on 22 salts or solutes such as $NH_4^+H_2PO_4^-$, $H_2NC{=}O$, $H_3C-CH_2-NH_3^+Br^-$, and $(H_2N)_2C{=}NH_2^+I^-$ (Wyckoff, 1962; Garbassi, Giarda & Fagherazzi, 1972; Adams & Small, 1973). Table 5 summarizes average values of the N-to-Y distance for each of the four choices of Y atom, along with the Ladd (1968) and Pauling (1960) ionic radii for each Y atom. Subtracting the Y radius from the $-$N-to-Y distance yields an estimate of the effective radius of $-N-H$ in a hydrogen bond $-N-H\cdots Y-$. The resulting calculated $-N-H$ radius varies only slightly with choice of Y (columns 4 and 6 of Table 4). In the hydrogen bond $-N-H\cdots O-$ the $-N-H$ radius is 1.54 Å (calculated from the Ladd oxygen radius), or 1.39 Å (calculated from the Pauling oxygen radius), compared to a van der Waals radius of 2.03 Å used in the CPK models. Thus, $-N-H$ adjacent to oxygen is actually shorter by $2.03-1.54=0.49$ Å (taking the Ladd values) or by $2.03-1.39=0.64$ Å (taking the Pauling values) than one measures from CPK models.

2. Next, the sides a, b, and c of the smallest rectangular box that could contain each cation were measured from modified CPK models in which each hydrogen that could form an H-bond (i.e., each proton covalently bonded to N or O, as well as the sulfhydryl proton of $H_3N^+-CH_2-CH_2-SH$) was either 0.49 or 0.64 Å smaller than in conventional CPK models. Table 5 gives the resulting "Ladd" and "Pauling" dimensions for comparison with the van der Waals dimensions.

3. For each cation and each of the three sets of dimensions, we calculated six alternative molecular radii: $r_1 \equiv \sqrt[3]{abc/8}$, the half-side of the cube with the same volume; $r_2 \equiv (a+b+c)/6$, the average half-side; $r_3 \equiv \sqrt[3]{ab/4}$ and $r_4 \equiv (a+b)/4$, where a and b are taken as the two shortest sides (in effect, r_3 and r_4 assume that steric restriction to a permeating cation depends on its smallest cross-section and is independent of its longest dimension); and r_5 and r_6, which differ from r_3 and r_4 only in that a and b are taken as the two longest sides for the three branched secondary amines,

$$(H_3C)_2NH_2^+,\quad H_3C-NH_2^+-CH_2-CH_3,\quad \text{and}\quad \begin{matrix} H_2C \diagdown \\ \quad\quad | \quad \diagup NH_2^+. \\ H_2C \end{matrix}$$

The experimental S_X values from Table 3 were then plotted against molecular radius in 18 alternative ways, permuting the six definitions of radius with the three sets of dimensions. Fig. 7 used r_2 and van der Waals dimensions, while Fig. 8 uses r_5 and Ladd dimensions.

Table 4. Calculation of effective radius of $-NH\cdots$ in a hydrogen bond

H-bond	Bond length (Å)	Ladd radius (Å)		Pauling radius (Å)	
		Y^-	$-N-H^+$	Y^-	$-N-H^+$
$-N-H\cdots O-$	2.79 ± 0.02 (16)	1.25	1.54	1.40	1.39
$-N-H\cdots Cl-$	3.26 ± 0.19 (3)	1.70	1.56	1.81	1.45
$-N-H\cdots Br-$	3.42 ± 0.06 (2)	1.87	1.55	1.95	1.47
$-N-H\cdots I-$	3.71 (1)	2.12	1.59	2.16	1.55

The N-to-Y center-to-center interatomic distance in the group $-N-H\cdots Y-$ (i.e., the "hydrogen-bond length") was tabulated from published crystallographic data (Wyckoff, 1962; Garbassi *et al.*, 1972; Adams & Small, 1973) for 22 salts or solutes, where Y represents the electronegative atom O, Cl, Br, or I. (For example, the $-N-H\cdots Cl$-length in the aminoguanidine hydrochloride crystal $(H_2N)_2C{=}N(-NH_2)-H\cdots Cl^-$ is 3.13 Å (Wyckoff, 1962).) If one crystal contained several species of group $-N-H\cdots Y-$ with the same Y but different lengths, only the shortest length was tabulated. Column 2 gives the average distance for all crystals of each type $-N-H\cdots Y-$ named in column 1. The Ladd and Pauling ionic radii for Y^- are listed for each Y^- in columns 3 and 5, respectively (from Ladd, 1968, and Pauling, 1960). Effective Ladd or Pauling radii for $-N-H^+$ are calculated in columns 4 and 6, respectively, as the $-N-H\cdots Y$ value of column 2 minus the Y^- radius of column 3 or 5, respectively. Note that the calculated $-N-H^+$ radii vary only slightly with choice of Y^-.

4. Finally, the Renkin equation, Eq. (5), was fitted to each of the 18 plots, and the best-fit values of equivalent pore radius in frog and rabbit gallbladders and the sum-squared error were compared for the 18 fits. The metallic cations studied previously (Li^+, Na^+, K^+, Rb^+, Cs^+, and Tl^+: Moreno & Diamond, 1974*b*) were included in calculating all fits. For each choice of radius definition, the sum-squared error is highest for van der Waals dimensions but differs little between Ladd dimensions and Pauling dimensions. For each choice of dimensions the sum-squared error decreases in the sequence $r_4>r_2\geqq r_3>r_1>r_6>r_5$. The choices of r_5 and Ladd or Pauling radii give almost identically good fits and are better than other choices of molecular radius. Since the Ladd r_5 fit is insignificantly better (sum-squared error 0.157, *vs.* 0.158 for Pauling r_5), it is the one displayed in Fig. 8 and used in further calculations. It yields $R_{\text{rabbit}}=4.4$ Å, $R_{\text{frog}}=8.1$ Å. The calculated equivalent pore radii, however, differ little for the various choices of molecular radius, especially in the rabbit: all 18 estimates fall between 4.2 and 5.8 Å for R_{rabbit}, between 6.8 and 13.0 Å for R_{frog}.

Fig. 8, which is based on a detailed effort to calculate H-bond shortening, still does not completely succeed in eliminating residual scatter. Although the scatter in Fig. 8 is considerably less than in Fig. 7, which ignores H-bond shortening, the scatter in Fig. 8 is comparable to that of an $S_X+vs.-r_{-H}$ plot, which simplistically corrects for shortening by omitting donor protons entirely from radius calculations. Possible causes of the imperfections in our treatment include the following: 1. Differences between P_X/P_{Na} values in frog and rabbit gallbladders may be partly due to factors other than differences in field strength and pore radius. 2. Fig. 6 provides only an approximate method of eliminating species differences in P_X/P_{Na} due to differences in field strength.

Table 5. Ionic dimensions (Å)

	van der Waals			Ladd			Pauling		
	a	*b*	*c*	*a*	*b*	*c*	*a*	*b*	*c*
ammonium	3.40	3.70	3.70	3.32	3.32	3.32	2.96	2.96	2.96
methylamine	3.50	3.75	4.15	3.50	3.75	4.10	3.50	3.75	4.10
ethylamine	3.75	4.30	6.10	3.75	4.30	5.80	3.75	4.30	5.80
propylamine	3.80	4.20	7.00	3.80	4.20	6.85	3.80	4.20	6.80
allylamine	3.80	4.50	6.80	3.80	4.50	6.65	3.80	4.50	6.60
isopropylamine	4.70	5.60	6.20	4.70	5.40	6.20	4.70	5.30	6.20
t-butylamine	5.20	5.50	6.00	5.10	5.50	6.00	5.00	5.50	6.00
azirane	3.80	4.20	4.20	3.80	4.10	4.20	3.80	4.10	4.20
dimethylamine	3.75	4.20	6.10	3.75	4.10	6.10	3.75	4.10	6.10
methylethylamine	3.80	4.20	7.00	3.80	4.10	7.00	3.80	4.05	7.00
hydrazine	3.70	3.75	4.10	3.10	3.40	4.10	3.05	3.20	4.10
methylhydrazine	3.70	4.80	5.50	3.70	4.20	5.40	3.70	4.10	5.40
formamidine	3.80	4.50	6.05	3.80	4.00	5.50	3.80	3.75	5.25
acetamidine	3.70	6.00	6.00	3.70	5.00	5.60	3.70	4.80	5.40
guanidine	3.00	5.50	6.00	3.00	5.00	5.50	3.00	4.80	5.30
aminoguanidine	3.00	5.48	7.05	3.00	4.95	6.70	3.00	4.80	6.48
methylguanidine	3.75	5.50	6.90	3.75	5.10	6.70	3.75	5.00	6.50
biguanidine	4.40	6.00	7.40	3.95	5.50	6.90	3.85	5.35	6.75
triaminoguanidine	3.00	7.20	7.60	3.00	6.90	7.10	3.00	6.40	6.90
ethylenediamine	3.75	4.40	7.00	3.75	4.40	6.65	3.75	4.40	6.50
aminoethanethiol	3.80	4.50	7.15	3.80	4.50	7.00	3.80	4.50	6.76
trimethylamine	4.70	5.40	6.00	4.20	5.40	6.00	4.00	5.40	6.00
tetramethylamine	5.40	5.40	6.00	5.40	5.40	6.00	5.40	5.40	6.00
6-amino-1-hexanol	5.10	7.10	8.40	5.10	7.00	8.30	5.00	6.90	8.30
ethanolamine	3.80	4.60	6.40	3.80	4.50	6.00	3.80	4.50	5.60
methoxyethylamine	3.80	4.60	7.20	3.80	4.60	7.10	3.80	4.50	7.10
1,3-aminopropanol	3.80	5.30	6.10	3.80	5.20	6.00	3.80	5.20	6.00
1,2-aminopropanol	4.50	5.70	6.80	4.50	5.70	6.50	4.50	5.40	6.20
2,1-aminobutanol	5.00	5.80	8.40	4.80	5.20	8.25	4.60	5.50	8.00
2-amino-2-hydroxy-methyl-1,3-propanol	5.30	7.00	7.90	5.30	6.70	7.50	5.30	6.50	7.70
1-aminopentanol	5.10	6.10	7.70	5.10	5.80	7.70	5.00	5.80	7.60
choline	4.50	6.10	8.00	5.40	6.10	8.00	5.40	6.10	8.00
Li^+				1.72	1.72	1.72	1.20	1.20	1.20
Na^+				2.24	2.24	2.24	1.90	1.90	1.90
K^+				2.88	2.88	2.88	2.66	2.66	2.66
Tl^+				3.08	3.08	3.08	2.80	2.80	2.80
Rb^+				3.16	3.16	3.16	2.96	2.96	2.96
Cs^+				3.68	3.68	3.68	3.38	3.38	3.38

For the first 32 cations of this Table, the sides *a*, *b* and *c* (in Å) of the smallest rectangular box that could contain each cation were measured, either from unmodified CPK molecular models to yield "van der Waals" dimensions (columns 2–4), or from CPK models modified to take account of hydrogen-bond shortening and yielding "Ladd" or "Pauling" dimensions (columns 5–7 and 8–10; *see text* for details). The values for metallic cations in the last six rows are twice the Ladd (1968) or Pauling (1960) radii. All oxycations except choline and 2-amino-2-hydroxymethyl-1,3-propanol were measured in the conformation with an intramolecular hydrogen bond.

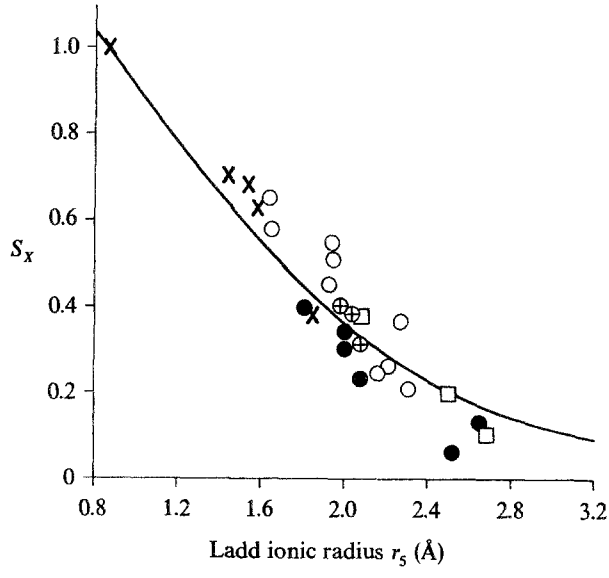

Fig. 8. As in Fig. 7 except that the radius of nitrogenous cations is taken as the Ladd radius r_5 as defined on p. 223 and calculated from Table 5. In effect, the van der Waals radii of the nitrogenous cations are shortened to take account of hydrogen bonding. With this choice of radius the experimental points show less scatter than in Fig. 7

3. The Renkin equation and our radius measurements remain a simplified and approximate treatment of steric effects. 4. Effective H-bond lengths in gallbladder tight junction may differ from H-bond lengths in the crystals on which Table 4 is based.

The meaning of the analysis of Tables 4–6 and Figs. 7 and 8 may be summarized in words as follows. Some of the differences between frog and rabbit gallbladders in P_X/P_{Na} values of the same nitrogenous cation can be interpreted as due to differences in field strength, as expressed in differing average P_{Na}/P_K values at the same pH (Fig. 5). When the effect of this difference is eliminated by using Fig. 6, the remaining differences are mainly a function of the cation's molecular radius (Figs. 7 and 8) and can be well fitted to a model based on steric restriction in which rabbit gallbladder has a narrower channel radius than frog gallbladder. By this criterion, cations with donor protons are seen by gallbladder tight junction as smaller than their van der Waals radius, and the apparent size reduction agrees with expectations based on formation of H-bonds with proton acceptors in the channel wall. As expressed in the superiority of the r_5 and r_6 fits, asymmetrical cations generally behave as if the steric restriction during permeation depends on the two shortest of their three dimensions, i.e. as if they traversed narrow parts of the channel with their long axis aligned with the direction of the channel. An exception is provided by three branched secondary

amines, which behave as if the two longest dimensions determine steric restriction (i.e., r_5 or r_6 fits superior to r_3 or r_4 fits). This may be due either to the orientation of the H-bond's dipole moment in the electric field across the membrane, or to constraints on orientation imposed by H-bonding between the cation's NH_2^+ group and the channel wall.

Analysis of Permeability Coefficients Corrected for Steric Effect

Our analysis of the "raw" permeability coefficients led to the dilemma (p. 215) that P's of nitrogenous cations depend both on H-bonds and on molecular size, and that the contributions of these factors to a set of P measurements in a gallbladder of one species alone are hard to unravel. In the preceding section, however, we saw that when those differences in permeability patterns between frog and rabbit gallbladders attributed to differences in field strength are eliminated by the procedure of Fig. 6, remaining species differences in permeability behave as if they are due largely to species differences in steric restrictions. The best fit to these species differences is obtained with values of equivalent pore radius of 4.4 and 8.1 Å in rabbit and frog gallbladder, respectively. We shall now correct the sets of P measurements in both species for steric restriction and analyze the corrected P's. This can be done by means of Fig. 9, which plots the Renkin ratio Y_X/Y_{Li} (from Eq. (4)) as a function of molecular radius for an equivalent pore radius of 4.4 or 8.1 Å, and which also plots the ratio of the Renkin ratios for pores of 4.4 and 8.1 Å radius, i.e. the predicted value of S_X (Eq. (5)).

For each cation in each species the single-species Renkin ratio Y_X/Y_{Li} (instead of the ratio $S_X \equiv (Y_X/Y_{Li})_{rabbit}/(Y_X/Y_{Li})_{frog}$, as used in Figs. 7 and 8) was calculated by inserting the cation's Ladd radius r_5 calculated from Table 4, plus the equivalent pore radius R ($=4.4$ Å in rabbit, 8.1 Å in frog) and Li^+'s Ladd radius (0.86 Å). Y_X/Y_{Li} may be read from Fig. 9. Y_{Na}/Y_{Li} was calculated similarly, and Y_X/Y_{Na} was then calculated as $(Y_X/Y_{Li})/(Y_{Na}/Y_{Li})$. The raw P_X/P_{Na} value from Table 3 was then divided by this Y_X/Y_{Na} value to give the corrected P_X/P_{Na} values of Table 3, abbreviated as $(P_X/P_{Na})'$. For most cations analyzed the correction factor is 1.5–3 in frog gallbladder, 3–12 in rabbit gallbladder. We have not attempted to extend the correction to larger solutes, since both the correction factor and the uncertainty in it become too large.

Fig. 10 plots values of $(P_X/P_{Na})'_{rabbit}$ against values for the same cations in frog gallbladder. $(P_X/P_{Na})'$ values in the two species are closely correlated. Most of the points in Fig. 10 lie above the line of 45° slope, whereas most points in the corresponding graph of raw P_X/P_{Na} values (Fig. 2) lie below

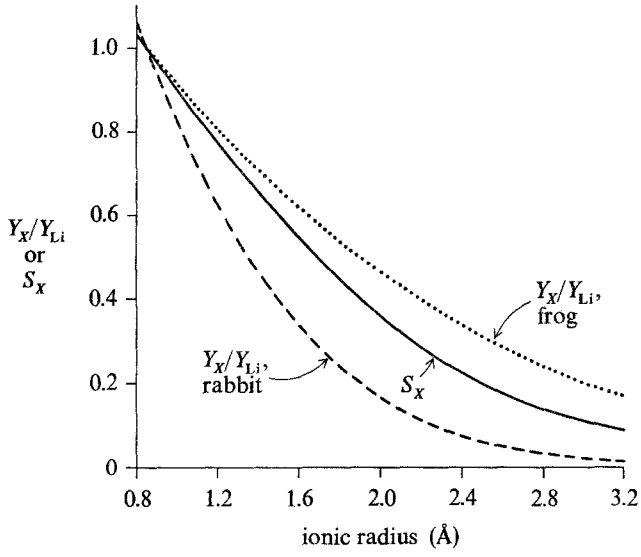

Fig. 9. The Renkin ratio Y_X/Y_{Li} calculated from Eq. (4) and plotted against cation radius r_X (Å). The equivalent pore radius R is taken as 4.4 Å or 8.1 Å (the best-fit value in rabbit or frog gallbladder: curve ------- or ·····, respectively), and r_{Li} is taken as the Ladd radius of 0.86 Å. In effect, these curves give, for each species and for a cation of Ladd radius given by the abscissa value, the ratio of the measured relative permeability coefficient P_X/P_{Li} to the value that would be observed in the absence of steric restriction. Curve ——— is the ratio of the ordinate values of curve ------ to curve ·····, i.e., the Renkin factor in rabbit divided by the factor in frog, or the value of S_X predicted by Eq. (5)

the line of 45° slope. This is because the equivalent pore radius is narrower in rabbit than in frog gallbladder, so that correction for steric effects increases P_X/P_{Na} values by a larger factor in rabbit than in frog. The slope of Fig. 10 is greater than 1. That is, after correction for the steric effect, rabbit gallbladder discriminates more sharply among cations than does frog gallbladder, as will also be demonstrated by Fig. 12 and discussed on p. 248.

Plots of $(P_X/P_{Na})'$ *vs.* (u_X/u_{Na}), *vs.* $\sqrt[3]{MW}$, or *vs.* the number of donor protons n_H still show that permeability depends on size ($\sqrt[3]{MW}$ or u_X/u_{Na}) as well as on n_H, even after correction for the steric effect. This is to be expected: if the permeation channel were of infinite width, permeability would depend upon mobility in the channel (which is presumably a decreasing function of molecular size) as well as on H-bond-dependent binding energies. Fig. 11 therefore plots the ratio $(P_X/P_{Na})'/(u_X/u_{Na})$, defined as P^*, against n_H for each species. Ordinate values for cations with the same n_H value still differ considerably. However, detailed examination of Fig. 11 reveals some patterns to these differences. For example, among cations with

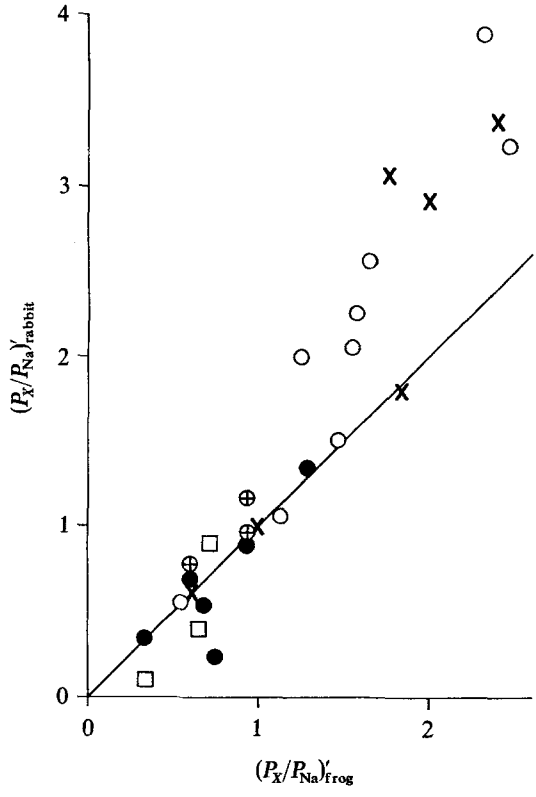

Fig. 10. Corrected P_x/P_{Na} values (i.e., $(P_x/P_{Na})'$) for 21 nitrogenous cations and six metallic cations in rabbit gallbladder (ordinate), plotted against values for the same cations in frog gallbladder (abscissa). Numbers and symbols are as in Fig. 2. The line is the line of identity. This figure differs from Fig. 2 in that P_x/P_{Na} has been corrected for the effects of steric restriction, by dividing by the ratio of Renkin factors Y_x/Y_{Na}. Note that most points lie above the line of identity in Fig. 10 but below the line of identity in Fig. 2, because steric restriction is more marked in rabbit than in frog gallbladder. Note also that the range of ordinate and abscissa values is greater in Fig. 10 than in Fig. 2

$n_H \geqq 4$, the most permeant cation is the same in frog and rabbit (no. 13, $H_2N-CH_2=NH_2^+$), as is also the least permeant cation (no. 18, $H_2N-C(NH_2)-NH-C(NH_2)=NH_2^+$); the five most permeant cations in rabbit include five of the six most permeant cations in frog; and the three least permeant cations in frog include three of the four least permeant cations in rabbit. The three cations symbolized by ⊕, which nominally have $n_H \geqq 4$ but may effectively have only $n_H \sim 3$ because of intramolecular H-bonds, have P^* values towards the lower extreme of the range for cations with $n_H \geqq 4$, similar to or approaching values for cations with $n_H = 3$ (*see also* Fig. 14*a* and p. 232). Thus, while some of the apparent scatter in Fig. 11 probably

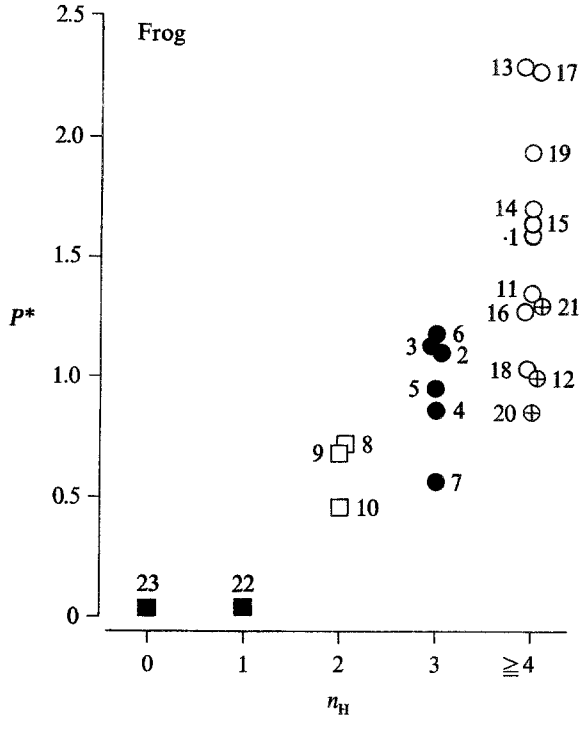

Fig. 11a

Fig. 11. Ordinate P^* defined as $(P_X/P_{Na})'$ (i.e., the permeability ratio corrected for steric restriction) divided by the free-solution mobility ratio u_X/u_{Na}. Abscissa, number of donor protons n_H. (*a*) Frog gallbladder; (*b*) rabbit gallbladder. Symbols and numbers as in Fig. 4. This figure differs from Fig. 4 in that P_X/P_{Na} has been replaced by $(P_X/P_{Na})'$

represents experimental errors and uncertainty in the steric correction, some of the scatter is meaningful and depends on detailed properties of the solute (*see* p. 244). Evidently, prediction of a cation's permeability from its n_H, u_X/u_{Na}, and ionic radius yields only a first approximation.

In Fig. 12 we have averaged values of log P^* for all solutes with the same value of n_H in a given species, and plotted the resulting average log P^* values against n_H. The apparent equality of log P^* at $n_H = 0$ and 1 is artifactual: at both n_H values P_X/P_{Na} is too low to detect experimentally and is arbitrarily assigned a value of 0.02 (the limit of experimental measurement) to avoid logarithms of zero. The most striking feature of Fig. 12 is that log P^* increases approximately linearly with n_H between $n_H = 1$ and 4 but then remains constant up to at least $n_H = 9$. That is, permeability increases with number of donor protons up to 4, but the channel behaves as if addition of donor protons beyond four fails to increase permeability further

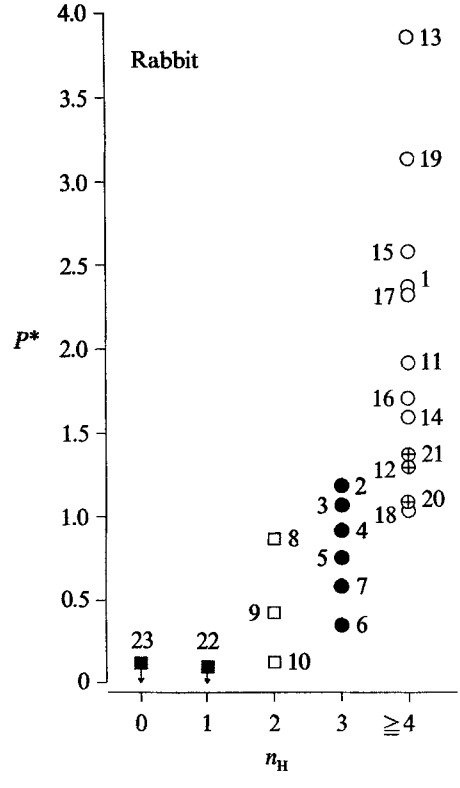

Fig. 11b

(*see* p. 240). The slope of the (log P^*) $-$ *vs.* $-n_H$ relation between $n_H = 1$ and 4 is steeper for rabbit gallbladder than for frog gallbladder, in agreement with the conclusion drawn from the slope of Fig. 10 that rabbit gallbladder discriminates more sharply among cations than does frog gallbladder. As discussed on p. 248, the slope of Fig. 12 would be approximately proportional to the difference between H-bond energies in the membrane and in water, if mobility ratios in the membrane (after correcting for steric restriction) and in water were similar.

Oxycations

Of the nitrogenous cations whose P_X/P_{Na} values have been measured and listed in Table 3, we have so far excluded two groups from analysis: lipid-soluble cations, discussed separately on pp. 233–239, and permeant oxycations (cations containing an oxygen atom). Of the 11 oxycations studied, two (H_3N^+-OH and $H_3C-NH_2^+-OH$) have relatively high P_X/P_{Na} values (1.41 and 0.98, respectively, in rabbit; 1.63 and 0.74, respectively, in frog). The points corresponding to these two cations are fairly close to those of other cations analyzed in Figs. 2–4 and 7–10, except that $(P_X/P_{Na})'$ for $H_3C-NH_2^+-OH$ in frog gallbladder is higher than expected for a cation with $n_H = 3$. The

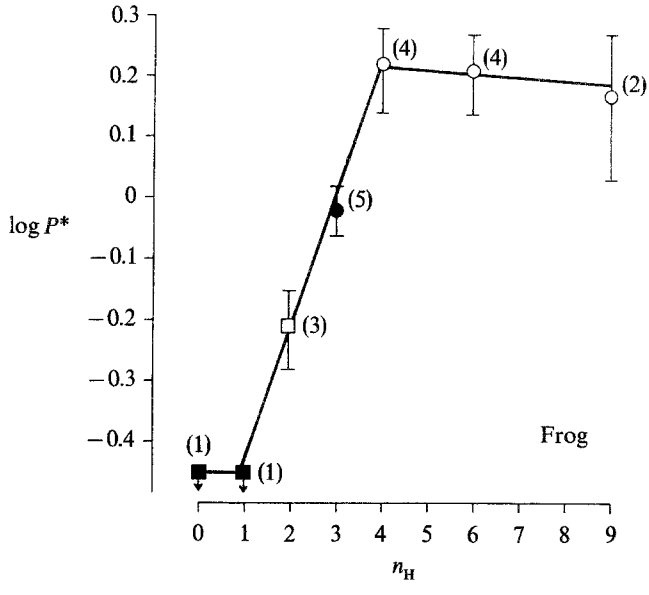

Fig. 12a

Fig. 12. Average value ±SEM of log P^* (ordinate), as a function of the cation's number of donor protons. (*a*) Frog gallbladder; (*b*) rabbit gallbladder. Beside each point is written in parentheses the number of cations studied. Cations with $n_H = 5$, 6 or 7 are averaged and presented as $n_H = 6$. This figure differs from Fig. 11 in that the ordinate is logarithmic and gives average values for many cations, and in that abscissa values of $n_H \geqq 4$ are split into three groups of $n_H = 4$, 5–7, and 9. Note that log P^* increases with n_H between $n_H = 1$ and 4, that the slope is steeper for rabbit than for frog, and that log P^* does not increase beyond $n_H = 4$

pK_a value of these two cations, 6, is sufficiently low that the possibility of an effect of the neutral form on the P_X/P_{Na} value (pp. 205–207) cannot be excluded. Thus, it seems unwise to attempt to interpret the P_X/P_{Na} values of these two cations.

The remaining nine oxycations (numbers 24 and 27–34 in Table 3) pose a clearly defined puzzle. All nine have low permeabilities ($P_X/P_{Na} \leqq 0.25$ in both rabbit and frog for all nine, <0.15 for eight). On a graph of $(P_X/P_{Na})'_{rabbit}$ *vs.* $(P_X/P_{Na})'_{frog}$, seven of these cations deviate far above the pattern defined by other cations (Fig. 13), meaning either that $(P_X/P_{Na})'_{rabbit}$ is unusually high or that $(P_X/P_{Na})'_{frog}$ is unusually low. The same conclusion follows from their deviating above the main pattern of a graph (not shown) of S_X against radius, similar to Fig. 8.

Examination of a graph of P^* for frog against n_H (Fig. 14*a*) shows that the positions of oxycations are not unusual, once one has taken account of the fact that the effective n_H value is 1 less than the number of protons bonded to O or N, because of intramolecular H-bonding

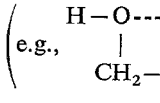

The corresponding graph for rabbit (Fig. 14*b*), however, shows that the oxycations that are most deviantly high in Fig. 13 are also deviantly high in Fig. 14*b*. Thus, what is

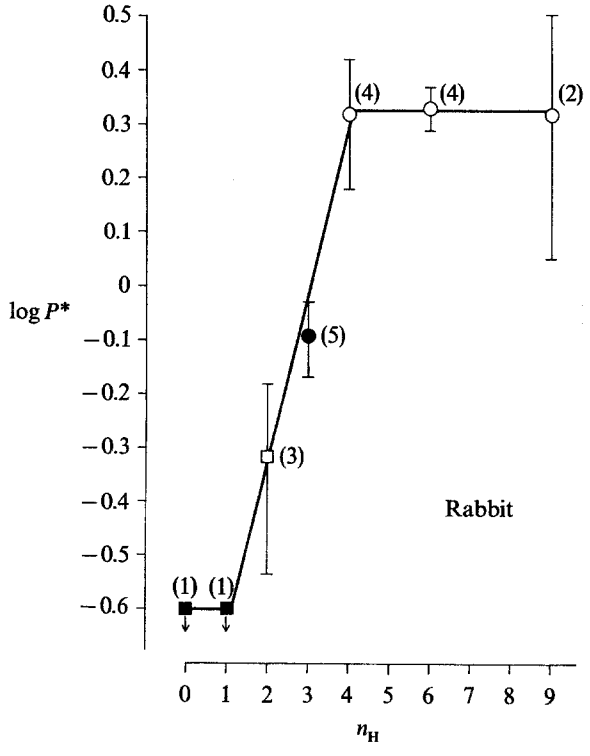

Fig. 12b

peculiar about oxycations is that they behave like other cations in frog but are more permeant than other cations in rabbit.

We suggest tentatively that the enhanced permeability of oxycations in rabbit gallbladder is because they can permeate via polar pathways in epithelial cell membranes as well as via tight junctions, as suggested by differences between rabbit and frog gallbladders in their nonelectrolyte permeability patterns. Whereas most nonelectrolytes permeate rabbit gallbladder in proportion to their lipid/water partition coefficient and presumably via the lipid bilayer portion of epithelial cell membranes, small hydrophilic nonelectrolytes permeate more rapidly than expected on this basis, as if they also had access to polar pathways through cell membranes (Wright & Diamond, 1969; Diamond & Wright, 1969*a*; Smulders & Wright, 1971; Moreno, 1975*b*). For small polyhydroxy nonelectrolytes such as $HO-CH_2-CH_2-OH$, this extra component of permeability is especially marked, as if the pore wall contained proton donors (such as $-NH_2$) and were preferentially permeable to proton acceptors. Most nitrogen atoms in the cations we have studied bear a partial positive charge and would therefore be less effective as proton acceptors than are oxygen atoms. In frog gallbladder this extra component of permeability to small hydrophilic nonelectrolytes is virtually absent, as if the polar pathways in the epithelial cell membranes were few or tight (Hingson & Diamond, 1972; Moreno, 1975*b*).

Lipid-soluble Cations

So far, the discussion has been confined to relatively hydrophilic cations—i.e., cations with up to only three carbons or with many hydrogen-bonding groups or with

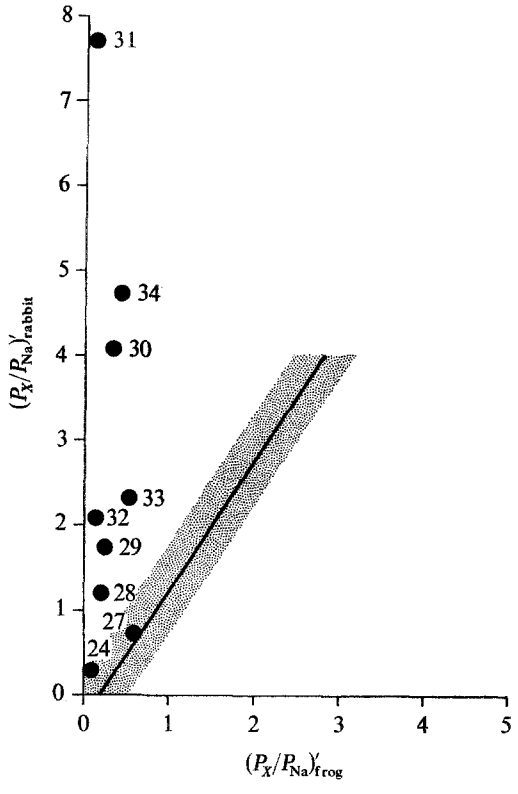

Fig. 13. Comparison of oxycation permeabilities corrected for steric restriction (i.e., $(P_X/P_{Na})'$), in rabbit (ordinate) and frog (abscissa) gallbladders. The straight line is the regression line, and the shaded area is the approximate envelope, of points for cations other than oxycations, from Fig. 10. The points represent values for nitrogenous cations that contain oxygen [nos. 27–34 from Table 3, but not 25 or 26 (*see text* p. 232) or 24 (because P_X/P_{Na} is immeasureably low)]. Note that most points for oxycations deviate far above the pattern for other cations, due to the unusually high $(P_X/P_{Na})'$ values for rabbit gallbladder documented in Fig. 14*b*

both. Such cations would be expected to have low solubility in membrane lipid. Their permeability pattern is consistent with the expectation of permeation predominantly via tight junctions, except (in rabbit) for oxycations, which may also permeate via polar pathways in epithelial cell membranes. We now consider lipid-soluble cations – i.e., cations with four or more carbons and with three or fewer donor protons (nos. 35–52 in Table 3).

Fig. 15 plots P_X/P_{Na} against number of carbons n_C for the alkylammonium cations studied ($R-NH_3^+$, $R_2NH_2^+$ or $R-NH_2^+-R'$, R_3NH^+, R_4N^+). With increasing n_C, P_X/P_{Na} in rabbit gallbladder (Fig. 15*a*) initially decreases, passes through a minimum around $n_C=3$, and then increases. The pattern in frog (Fig. 15*b*) differs in that the increase in P_X/P_{Na} with n_C for $n_H=1$ is less steep than in rabbit, and in that for $n_H=2$ or 3 P_X/P_{Na} apparently decreases with increasing n_C towards a constant value rather than passing through a minimum.

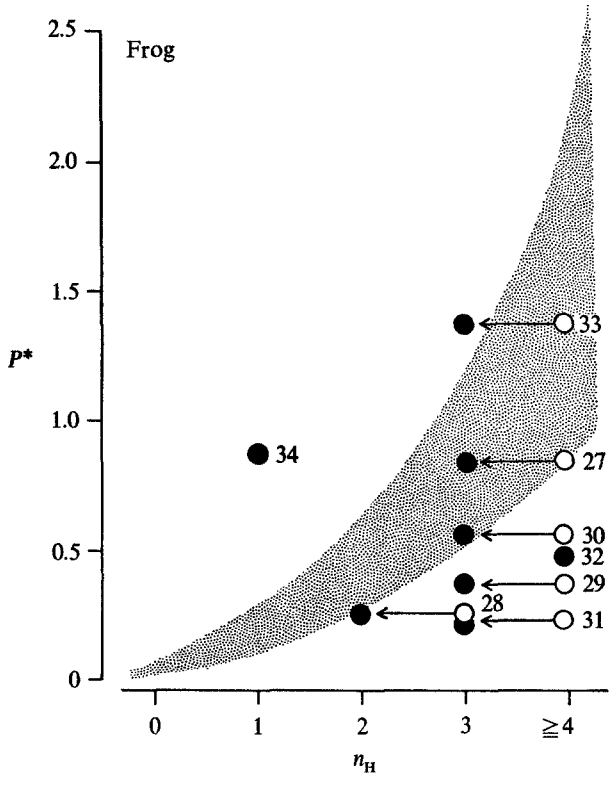

Fig. 14a

Fig. 14. (*a*) The experimental points give P^* (ordinate) as a function of n_H (abscissa) for oxycations in frog gallbladder. Values for oxycations that can form intramolecular H-bonds are plotted twice and connected by an arrow: on the right (points ○), at an n_H value corresponding to the nominal number of donor protons, whether or not the protons take part in intramolecular H-bonds; on the left (points ●, as for other oxycations), at an n_H value corresponding to the number of donor protons actually available to proton acceptors on membrane sites and not involved in intramolecular H-bonds. The shaded area is the approximate envelope of points for cations other than oxycations, from Fig. 11*a*. If the possibility of intramolecular H-bond formation is ignored (points ○), permeabilities of some oxycations seem deviantly low, but they are closer to the pattern for other cations when intramolecular H-bonding is taken into account. (*b*) Same as (*a*) but for rabbit gallbladder. The shaded area is the approximate envelope of points from Fig. 11*b*. Note the interrupted ordinate. Even after intramolecular H-bonding has been taken into account, permeabilities of oxycations are higher than expected from the pattern for other cations

Fig. 15*a* is strikingly similar to the permeability pattern in gallbladder, erythrocyte, mitochondria, and the alga *Nitella* for several series of nonelectrolytes, such as alkyl amides, alkyl ureas, and dihydroxy alkyl alcohols (Collander, 1954; Tedeschi & Harris, 1955; Wright & Diamond, 1969; Galey, Owen & Solomon, 1973; Naccache & Sha'afi, 1973). In these cases the minimum in permeability as a function of chain length has been

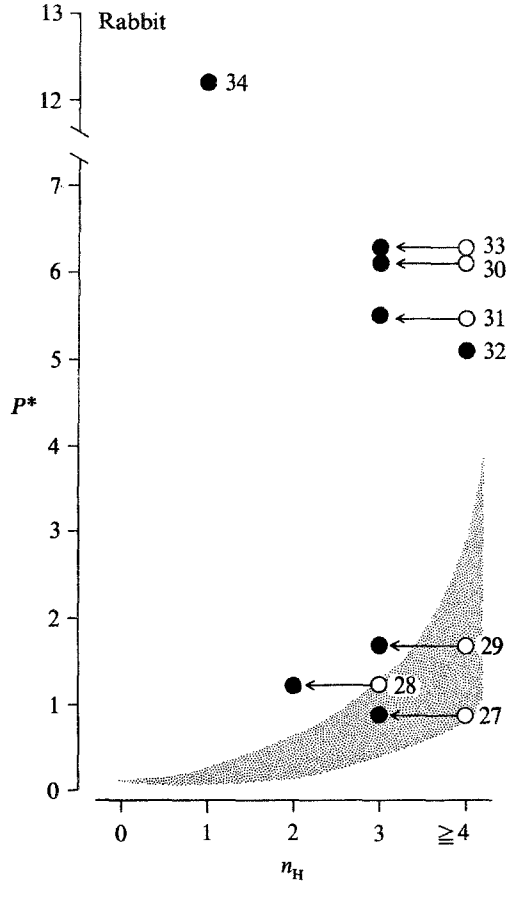

Fig. 14b

interpreted in terms of two parallel permeation routes: permeation through membrane lipid, where permeability increases with increasing lipid-to-water partition coefficient, hence with increasing chain length; and permeation through hydrophilic channels, where permeability decreases with increasing size, hence with increasing chain length. By analogy, Fig. 15*a* probably means that in rabbit gallbladder the small hydrophilic cations permeate mainly via tight junctions (where P_X/P_{Na} decreases with chain length), the larger lipid-soluble cations mainly via epithelial cell membrane lipid (since conductance of primary amines in an artificial lipid bilayer increases with amine chain length, as shown by J. Moreno & G. Szabo (*unpublished observations*)). The flattening of graphs of P_X/P_{Na} *vs.* n_C curves in frog (Fig. 15*b*) suggests that membrane lipid is less permeable in frog gallbladder than in rabbit gallbladder, so that, for $n_C > 3$, with increasing n_C the decrease in permeation via tight junctions approximately offsets the increase in permeation via membrane lipid.

Comparison of P_X/P_{Na} for branched and straight-chain isomers with the same n_H and with $n_C \geqq 4$ shows that the branched isomer is always the less permeant one in

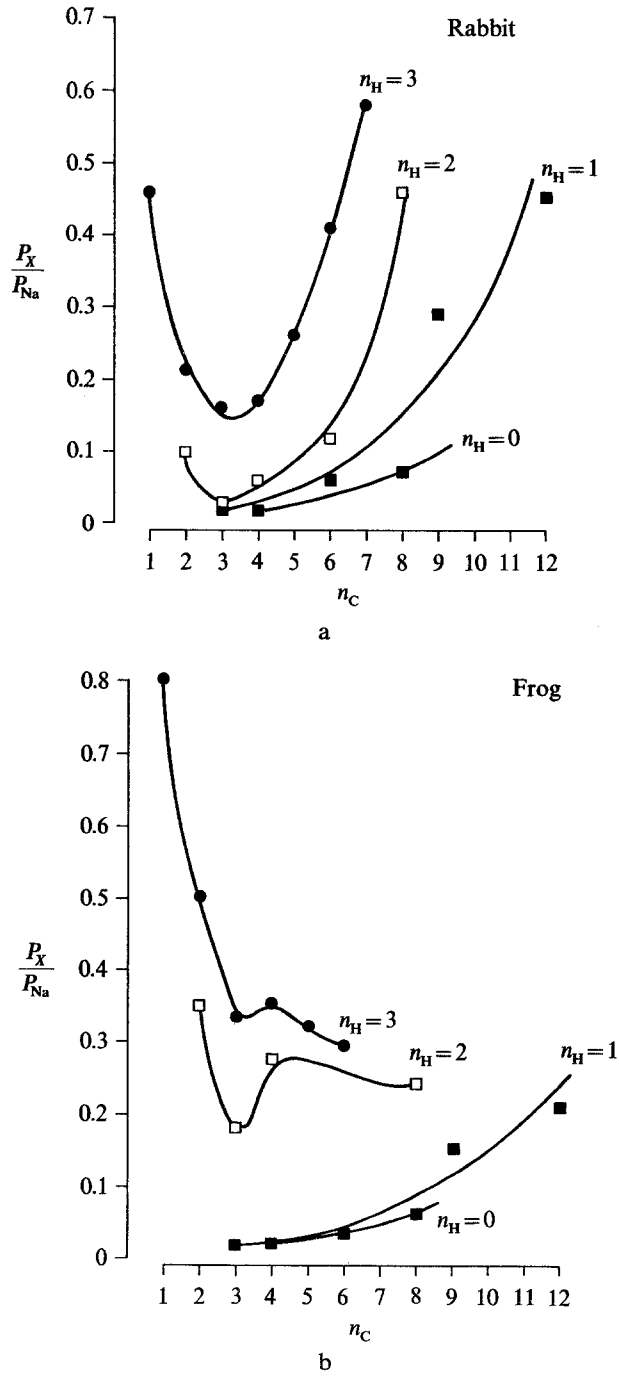

Fig. 15. (*a*) P_X/P_{Na} of alkylammonium cations in rabbit gallbladder, as a function of number of carbon atoms n_C. Symbols as in Fig. 2. Points representing cations with the same number of donor protons n_H are connected. Only cations with saturated unbranched carbon chains and lacking functional groups other than a single amino group are included. Note that P_X/P_{Na} passes through a minimum near $n_C=3$ but increases with n_H for any n_C value. (*b*) Same as (*a*) but for frog gallbladder

rabbit and is usually so in frog. For example, P_X/P_{Na} in rabbit is

lower for $H_3C-\underset{\displaystyle CH_3}{\overset{\displaystyle CH_3}{\overset{|}{\underset{|}{C}}}}-NH_3^+$ than for $H_3C-CH_2-CH_2-CH_2-NH_3^+$,

lower for $H_3C-\underset{\displaystyle CH_3}{\overset{|}{CH}}-CH_2-CH_2-NH_3^+$

than for $H_3C-CH_2-CH_2-CH_2-CH_2-NH_3^+$,

lower for $H_2C\begin{matrix}\diagup CH_2-CH_2\diagdown \\ \diagdown CH_2-CH_2\diagup\end{matrix}CH-NH_3^+$

than for $H_3C-CH_2-CH_2-CH_2-CH_2-CH_2-NH_3^+$, and

lower for $(H_3C-\underset{\displaystyle CH_3}{\overset{|}{CH}}-CH_2-)_2NH_2^+$ than for $(H_3C-CH_2-CH_2-CH_2-)_2NH_2^+$.

The same finding has often been reported for nonelectrolyte permeation through membrane lipid (e.g., Collander, 1954; Wright & Diamond, 1969; Hingson & Diamond, 1972; Galey, Owen & Solomon, 1973; Naccache & Sha'afi, 1973; Wright & Pietras, 1974) and for nonelectrolyte partition into membrane lipid (Diamond & Katz, 1974; Lange, Gary-Bobo & Solomon, 1974). The suggested interpretation is that more work is required to insert a branched solute than a straight solute into the ordered array of hydrocarbon chains of a lipid bilayer.

The effect of temperature on P_X/P_{Na} was compared in each species for three types of cations: (a) Cations of very low lipid solubility, such that permeation is largely via tight junctions, and sufficiently small that the value of their steric factor S_X in the tight junctions should be similar to that for Na^+ (NH_4^+ studied in rabbit, NH_4^+ and K^+ in frog). (b) Cations of low lipid solubility such that permeation is largely via junctions, but considerably larger than Na^+ ($H_3C-NH_3^+$ in rabbit, $H_3C-CH_2-NH_3^+$ in frog). (c) Cations that are quite lipid-soluble, too large to permeate via junctions, hence likely to permeate mainly via membrane lipid ($(H_3C-CH_2-CH_2-CH_2-)_3NH^+$ in rabbit, $(H_3C-CH_2-CH_2-)_3NH^+$ in frog). As summarized in Table 6, the temperature coefficient Q_{10} of P_X/P_{Na} in both species is highest for the lipid-soluble cations of type c, lower for the sterically restricted hydrophilic cations of type b, and lowest for the small hydrophilic cations of type a. This pattern for cation permeation duplicates a familiar finding for nonelectrolyte permeation: lipid-soluble nonelectrolytes that permeate via membrane lipid show steeper temperature dependence of permeability than small hydrophilic solutes that permeate via hydrophilic channels, in gallbladder, erythrocyte, and several algae (Wartiovaara, 1942, 1956; Wright & Diamond, 1969; Hingson & Diamond, 1972; Galey, Owen & Solomon, 1973). Among hydrophilic cations the higher Q_{10} for larger cations may be due to greater fluctuation in pore size at higher temperature (for a similar finding in a cation exchange resin *see* Sherry's (1969) discussion of La^{3+} exchange by the resin Line Y).

For nonelectrolytes that permeate via membrane lipid, permeability decreases with increasing number of hydrogen bonds, because the solute's partition coefficient in the membrane is lowered by hydrogen bonding in the aqueous phase (Collander, 1949; Diamond & Wright, 1969*a*, *b*; Diamond & Katz, 1974). For the cations listed in

Table 6. Effect of temperature on cation permeation in gallbladder

(a) *Frog gallbladder*

Cation X	P_X/P_{Na}		Q_{10}	E (kcal/mole)
	5 °C	23 °C		
NH_4^+	2.05 ± 0.03 (4)	1.82 ± 0.02 (4)	1.6	7.8
K^+	1.56 ± 0.03 (4)	1.52 ± 0.05 (4)	1.7	8.5
$H_3CCH_2NH_3^+$	0.44 ± 0.04 (4)	0.49 ± 0.03 (4)	1.8	9.7
$(H_3CCH_2CH_2)_3NH^+$	0.08 ± 0.04 (4)	0.15 ± 0.05 (4)	2.6	15.5

(b) *Rabbit gallbladder*

Cation X	P_X/P_{Na}		Q_{10}	E (kcal/mole)
	7 °C	23 °C		
NH_4^+	1.48 ± 0.14 (3)	1.40 ± 0.05 (3)	1.7	9.0
$H_3CNH_3^+$	0.50 ± 0.03 (3)	0.68 ± 0.03 (3)	1.9	11.2
$(H_3CCH_2CH_2CH_2)_3NH^+$	0.34 ± 0.01 (3)	0.53 ± 0.05 (3)	2.0	11.9

Each entry is the mean ± SEM (number of observations) of P_X/P_{Na} measurements in frog and rabbit gallbladders at the temperatures indicated. From the change in P_X/P_{Na} with temperature, each cation's Q_{10} value in column 4 and activation energy E in column 5 was calculated on the assumption that Q_{10} for P_{Na} is 1.72 over this temperature range (Barry *et al.*, 1971).

Table 3, the pattern is more complex. The presence of an additional H-bonding group does lower P_X/P_{Na} for $H_3C-CH_2-CH(NH_3^+)-CH_2OH$ compared to $H_3C-CH_2-CH(NH_3^+)-CH_3$, for $HO-CH_2-(CH_2)_4-NH_3^+$ compared to $H_3C-(CH_2)_4-NH_3^+$, and for $HO-CH_2-(CH_2)_5-NH_3^+$ compared to $H_3C-(CH_2)_5-NH_3^+$. However, Fig. 16 also makes it obvious that when one compares primary, secondary, tertiary, and quaternary amines, P_X/P_{Na} *increases* with n_H for the large lipid-soluble cations just as for the smaller hydrophilic cations. This finding is duplicated for the conductance of primary and secondary amines in lipid bilayers (J. Moreno & G. Szabo, *unpublished observations*). This may suggest that, as an intermediate step in permeation, the cation is located with its lipophilic tail buried in the bilayer's hydrocarbon tails and its amine group among the bilayer's polar head groups or towards the aqueous solution.

Discussion

In this section we shall discuss in turn the contributions that hydrogen bonds, steric restriction, and electrostatic forces make to nitrogenous cation discrimination by gallbladder tight junction. We shall then compare cation discrimination by gallbladder with cation discrimination by other selective systems, such as nerve's sodium channels and artificial carriers and channels.

Effect of Hydrogen Bonding

The permeability of ion-selective channels of gallbladder tight junctions to nitrogenous cations, including amines in the charged form, *increases* with increasing hydrogen-bonding ability of the cations. This pattern is exactly the opposite of the gallbladder pattern for permeation of amines in the uncharged form and most other nonelectrolytes: their permeability *decreases* with increasing hydrogen-bonding ability of the solute (Diamond & Wright, 1969*a*, *b*). Lipid-soluble nonelectrolytes presumably cross gallbladder epithelium via the cell membranes rather than via the tight junctions, and a similar inverse relation between permeability and H-bonding ability is observed for membranes of single cells and for lipid bilayers. Because lipid membranes contain many fewer H-bonding groups than does water, H-bonding ability of the solute shifts the solute's partition equilibrium between membrane and water in favor of water, thereby reducing the solute's membrane concentration and hence permeability.

Evidently, then, the channels of gallbladder tight junctions contrast with lipid bilayers in that the former do contain numerous H-bonding sites, whose properties are responsible for nitrogenous cation selectivity. The permeability pattern (permeability increasing with the solute's proton-*donor* ability) suggests that tight junctions contain proton acceptors that discriminate more markedly among solutes of differing proton-donor ability than does water. Since carboxyl or phosphate groups, which are implicated as the sites controlling alkali cation permeation (Moreno & Diamond, 1974*b*), are strong proton acceptors, and since variation in field strength of membrane sites appears to modulate permeability for nitrogenous cations (Fig. 5 and pp. 215–217) as well as for alkali cations (Moreno & Diamond, 1974*b*), the postulated proton-acceptor sites are probably identical with the sites controlling alkali cation permeability. It will be recalled that addition of donor protons beyond four to a solute fails to increase permeability further (Fig. 12). This suggests either that the sites can form only four H-bonds with proton donors, and that further protons on a solute remain H-bonded to water in the permeation channel; or else that the sites can accept more than four protons, but that only for the first four protons does the site discriminate more sharply than does water.

To make this model explicit, we represent a cation's permeability coefficient P by an expression[5] of the form (Eisenman, 1965*b*):

$$P = K u^*. \tag{6}$$

5 Eq. (6) is a highly simplified representation: permeating ions surely encounter a series of energy barriers and wells, such that K and u^* vary with position in the membrane (e.g. *see* Parlin & Eyring, 1957; Hille, 1975).

Here u^* represents the solute's mobility in the membrane, while K is the solute's partition coefficient between water and membrane (concentration in membrane divided by concentration in water), or the solute's binding constant (referred to water) to membrane sites. K is related to free energies of solution or binding by the expression

$$-RT \ln K = \Delta F_{\text{transfer}} = \Delta F_{\text{ion/site}} - \Delta F_{\text{hydration}} \tag{7}$$

where $\Delta F_{\text{hydration}}$ is the cation's hydration energy, $\Delta F_{\text{ion/site}}$ its attraction energy to membrane sites (mainly due to H-bond forces, which include electrostatic forces), and $\Delta F_{\text{transfer}}$ the free-energy change in transferring the cation from water to the membrane sites. Combination of Eqs. (6) and (7) yields

$$\ln(P/u^*) = -\Delta F_{\text{transfer}}/RT. \tag{8}$$

Recall now that the calculation of $(P_X/P_{\text{Na}})'$ $(= P^* u_X/u_{\text{Na}})$ from (P_X/P_{Na}) attempts to remove effects of steric restriction, which may affect K, u^*, or both. Thus, Eq. (8) shows that P^*, the ordinate of Fig. 12, would be proportional to $-\Delta F_{\text{transfer}}$ if values of u^* (mobilities in the channel) after correction for steric restriction were proportional to values of u (mobilities in free solution). This condition need not be valid: the H-bond forces and electrostatic forces expressed in K may also cause nonproportionality between u^* and u.

When we say that the membrane contains proton acceptors which discriminate more markedly among solutes of differing proton-donor ability than does water, we mean the following: for two solutes a and b, b having more donor protons than a, the *difference* between the binding energies in the membrane is greater than the *difference* in water (i.e., $\Delta F_{b,\text{site}} - \Delta F_{a,\text{site}}$ more negative than $\Delta F_{b,\text{hydration}} - \Delta F_{a,\text{hydration}}$, but $\Delta F_{b,\text{site}}$ need not be more negative than $\Delta F_{b,\text{hydration}}$). Then the membrane/water partition coefficient K will be larger for the solute b with more donor protons. Increased solute/membrane forces will not only increase the solute's concentration but also reduce its mobility in the membrane. In analogy with most other systems, however (Diamond & Wright, 1969*b*, pp. 609–612; Moreno & Diamond, 1975, pp. 58–63), increased solute/membrane forces presumably increase the solute's partition coefficient by a factor larger than the factor by which the solute's mobility in the membrane is reduced. Thus, the net effect is that the solute with more donor protons has the higher permeability.

Since the H-bonding ability of water is responsible for some of water's most distinctive properties as a solvent, some readers may be surprised

that sites in gallbladder tight junction discriminate even more sharply among proton donors than does water. However, this discrimination is duplicated by several model systems. For example, Krishnan and Friedman (1970) compared enthalpies of solution for alkylammonium ions with varying numbers of donor protons in the solvents water, dimethyl sulfoxide, and propylene carbonate. As with water, the structures of the latter two solvents include oxygen atoms that function as proton acceptors in hydrogen bonds. The negative change in enthalpy of solution with each additional donor proton – i.e., the incremental enthalpy $\delta \Delta H$ of solution and of H-bond formation of a donor proton – was found to be larger for dimethyl sulfoxide and propylene carbonate than for water. Thus, a "membrane" of either of these two solvents interposed between two aqueous phases would resemble gallbladder in its preferential permeability to proton-rich cations.

H-bonds affect permeability not only by increasing cation/site binding energies, as discussed in the preceding four paragraphs, but also in the entirely different way discussed on pp. 221–226: H-bonding solutes behave in an H-bonding environment as if smaller than their van der Waals radius, and therefore encounter less steric restriction. This latter effect was first recognized clearly and discussed in detail for cation permeation in nerve's Na^+ channel by Hille (1971), who considered this steric contraction effect to be the main reason for the increase in cation permeability with proton-donor ability. Hille reasoned that the first effect (the binding energy effect) could not be significant in determining cation selectivity, because "it would be difficult for the channel to provide as adaptable and as concentrated a hydrogen bonding environment as water provides" (Hille, 1971, p. 613). The steric contraction effect is indeed important in gallbladder, as discussed on pp. 221–226. Nevertheless, even after correction of permeability coefficients for steric effects, permeability still increases with number of H-bonds (Fig. 12) because of the binding-energy effect, which constitutes the principal reason for increase in permeability with proton-donor ability in gallbladder. As discussed in the preceding paragraph, the hydrogen-bonding environment of some model systems does discriminate more sharply among proton donors than does water, and this is also probable for the gallbladder permeation channel.

Steric Restriction

Permeation through gallbladder tight junction exhibits a steeper size dependence than does diffusion in free solution. Figs. 7 and 8 and pp. 220–227 show that this effect is in good agreement with a model based on steri-

cally restricted diffusion, provided that one can first isolate the steric effect from other factors influencing permeability (Fig. 6) and that one considers the effect of H-bonding on molecular size.

It remains only to emphasize that the steric effect cannot be understood unless one also considers the H-bond binding-energy effect, since permeability depends upon H-bond binding energies as well as upon size. Thus, one could easily be misled about the permeability pattern if one studied only a small group of solutes in a single membrane. For example, if one compared only amines with the same number of donor protons, the parallel between permeability ratios and free-solution mobility ratios (Moreno & Diamond, 1974*a*, Fig. 1) might have been interpreted to mean that the gallbladder is completely nonselective. Again, if one compared only the successively substituted methyl ammonium cations NH_4^+, $H_3C-NH_3^+$, $(H_3C)_2NH_2^+$, $(H_3C)_2NH^+$, and $(H_3C)_4N^+$, the progressive decrease in permeability with increasing size might mislead one into attributing selectivity solely to molecular sieving in a narrow channel. It is a widespread practice in membrane biology to estimate the equivalent pore radius of a membrane roughly from the size of the smallest impermeant solute, or more accurately by fitting raw permeability coefficients as a function of molecular radius to the Renkin equation. The solutes used are often small hydrophilic nonelectrolytes, but ions have also been used. Often, the calculations tacitly assume permeability to be governed largely by size and only secondarily or negligibly by molecular interactions. This assumption may introduce gross errors. For instance, in frog gallbladder $(H_3C)_3NH^+$ is virtually impermeant, while $H_2N-NH^+=C(NH-NH_2)_2$, which is approximately twice as large (but has many more donor protons), is quite permeant ($P_X/P_{Na}=0.55$). Detailed examination of permeability patterns of small hydrophilic nonelectrolytes in gallbladder also reveals features that cannot be explained by size considerations alone (Wright & Diamond, 1969).

Isolation of steric effects from other factors influencing permeation may often prove complex. What has made a steric analysis possible in gallbladder is the availability of two membranes that are similar in most respects and different in a few ways – i.e., the possibility of comparing gallbladders of two animal species, differing in channel radius and in electrostatic field strength but apparently similar in the mechanism of ion permeation and the chemical type of cation-selective site. Our analysis based on the Renkin equation is obviously only an approximate one, since this equation assumes spherical solutes and right circular cylindrical pores with rigid and inert walls. Thus, stress should not be placed on the exact numerical values of the calculated pore radii.

Effects of Field Strength

Selectivity isotherms for nitrogenous cation permeation can be constructed from differences among individual animals in P_X/P_K values, and from effects of pH on P_X/P_K values (Fig. 5). These isotherms are very similar to the isotherms constructed previously for alkali cation permeation (Moreno & Diamond, 1974*b*). The alkali cation isotherms were consistent with the interpretation that pH-dependent variation and individual variation in P_X/P_K are mediated by variation in "field strength" of membrane sites, as discussed by Eisenman (1961, 1962, 1965*b*). According to this interpretation, variation in the partial negative charge on cation-binding sites in the membrane causes the electrostatic forces between cation and site to vary, hence alters $\Delta F_{\text{ion/site}}$ in Eq. (7) and hence alters relative permeability coefficients. The same interpretation may underlie the isotherms for nitrogenous cation permeation. In the case of the alkali cations, however, the availability of explicit predictions for the direction of the pH effect on P_X/P_K values, based on Eisenman's theoretical calculations of Coulomb forces, provided striking support for this interpretation. No such theoretical predictions are available for nitrogenous cations, since hydration energies of most nitrogenous cations are unknown, and since the problem of calculating electrostatic forces between a cation and an anion as a function of the anion's charge is far more complex when the cation is multipolar and of unknown charge distribution and polarizability (as true of most nitrogenous cations) than when the cation is monopolar and of low polarizability (as true of the alkali cations).

Field-strength effects may account for some of the differences in permeability observed among cations with similar n_H values and similar sizes (Fig. 11). In fact, a clear distinction cannot be drawn between H-bonds, on the one hand, and field-strength effects on ion-site electrostatic forces, on the other hand, since such electrostatic forces are one of the three types of attractive forces contributing to H-bond energies (footnote 2, p. 215). Throughout this paper we have simplistically correlated permeability with number of donor protons n_H, as if all H-bonds were of equal strength. More realistically, different H-bonds may be of different strengths, depending on the strength of the several component attractive forces, including electrostatic forces. Thus, one could also express the meaning of the permeability differences among cations with similar n_H values and sizes (Fig. 11) by saying that cations with similar n_H may still differ in the total energy of the H-bonds formed with a site. This view is supported by the observation that in both rabbit and frog gallbladders certain cations have high P^*

values, and other cations have low P^* values, compared to the mean value for cations of their n_H value and size.

Comparison of Nitrogenous Cation Selectivity Patterns in Different Systems

For comparison with nitrogenous cation selectivity patterns in gallbladder, Table 7 summarizes nitrogenous cation permeability ratios in the Na^+ channel of nerve determined by Hille (1971); ratios determined for the carriers nonactin, trinactin, valinomycin, and hexadecavalinomycin by Krasne and Eisenman (*personal communication*) and Eisenman and Krasne (1973); and ratios determined for the channel-forming antibiotic gramicidin by Krasne and Eisenman (*personal communication*). Further relevant data not tabulated in Table 7 include permeabilities of five cationic amines measured in glass electrodes by Eisenman (1965*a*, Fig. 39), and stimulatory or inhibitory effects of cationic amines on the enzymes pyruvate kinase and propanediol dehydratase (Krasne & Eisenman, *personal communication*, calculated from published data).

All eight systems summarized in Table 7 except hexadecavalinomycin (*see* footnote 6, p. 249) exhibit a correlation between permeability and number of donor protons. The correlation for frog and rabbit gallbladders was most clearly illustrated by Figs. 11 and 12, which plot $(P_X/P_{Na})'/(u_X/u_{Na}) \equiv P^*$, or else log P^*, against number of donor protons, after correction for the steric effect. While Table 7 simply presents P_X/P_{Na} values, not divided by u_X/u_{Na} values nor corrected for the steric effect, it is still clear that, for nonactin and trinactin, P_X/P_{Na} values are higher for all nitrogenous cations with $\geqq 4$ donor protons than for any nitrogenous cations with $\leqq 3$ donor protons. For nonactin, valinomycin, and gramicidin as for gallbladder, removal of each successive proton of NH_4^+ to form $H_3C-NH_3^+$, $(H_3C)_2NH_2^+$, and $(H_3C)_3NH^+$ progressively reduces permeability. For nerve, all nitrogenous cations with $\leqq 3$ protons have undetectably low permeabilities; only cations with $\geqq 4$ protons are detectably permeant.

Table 7 also makes it obvious that proton donor ability is not the sole factor in permeability, though it is surely an important one. In nerve, for instance, the three cations studied with > 7 protons are effectively impermeant. It is suggestive that in size these are the three largest of the proton-rich cations Hille (1971) studied, leading one to suspect that steric restrictions are operative in nerve as in gallbladder, as pointed out by Hille. Differences among different systems in steric restrictions may account for

Table 7. Comparison of organic cation permeabilities in eight systems

n	Solute	MW	Frog g.b.	Rabbit g.b.	Nerve	Nonactin	Trinactin	Valinomycin	HDVal	Gramicidin
$\geqq 4$	NH_4^+	18	1.73	1.42	0.16	1111	434	1000	45	5.45
	$H_2N-NH_3^+$	33	1.13	1.05	0.59	$\leqq 0.37$	$\leqq 0.10$	$\leqq 2$	1.6	2.90
	$HO-NH_3^+$	34	1.41	1.63	0.94	$\leqq 0.43$	$\leqq 0.11$	$\leqq 0.5$	1.1	5.15
	$H_2N-CH=NH_2^+$	45	1.31	1.03	0.14	$\leqq 56$	$\leqq 13$	$\leqq 150$	52	4.7
	$H_3C-NH-NH_3^+$	47	0.51	0.30	~ 0	—	—	—	—	—
	$H_2N-C(CH_3)=NH_2^+$	59	0.55	0.19	~ 0	—	—	—	—	—
	$(H_2N)_2C=NH_2^+$	60	0.94	0.70	0.13	$\leqq 14$	$\leqq 3.8$	$\leqq 17.5$	90	0.08
	$H_3C-NH-C(NH_2)=NH_2^+$	74	0.69	0.26	~ 0	—	—	—	—	—
	$H_2N-NH-C(NH_2)=NH_2^+$	75	0.89	0.57	0.06	—	—	—	—	—
	$HO-NH-C(NH_2)=NH_2^+$	76	—	—	0.12	$\leqq 142$	$\leqq 54$	$\leqq 250$	45	0.73
	$NH=C(NH_2)-NH-C(NH_2)=NH_2^+$	102	0.23	0.07	~ 0	—	—	—	—	—
	$H_2N-NH^+=C(NH-NH_2)_2$	106	0.55	0.28	~ 0	—	—	—	—	—
3	$H_3C-NH_3^+$	32	0.80	0.46	~ 0	$\leqq 0.14$	$\leqq 0.043$	8.8	210	0.73
	$H_3C-CH_2-NH_3^+$	46	0.50	0.21	—	$\leqq 0.28$	—	$\leqq 1.25$	—	0.04
2	$(H_3C)_2NH_2^+$	46	0.35	0.10	~ 0	$\leqq 0.011$	—	$\leqq 0.75$	—	0.02
1	$(H_3C)_3NH^+$	60	~ 0	-0	—	$\leqq 0.004$	—	$\leqq 0.125$	320	—
0	$(H_3C)_3N^+-CH_2-CH_2-OH$	104	~ 0	-0	~ 0	—	—	—	—	—
	$(H_3C)_4N^+$	74	~ 0	~ 0	~ 0	—	—	—	—	~ 0
	$(H_3C-CH_2)_4N^+$	130	~ 0	~ 0	~ 0	—	—	—	—	—
	$(H_3C)_3N^+(OH)CH_2$	122	~ 0	~ 0	~ 0	—	—	0.031	1300	—
	$(H_3C)_3N^+CH_2-CH_2-O-C(=O)-CH_3$	146	—	—	—	—	—	0.016	4500	—

n = number of protons available for H-bonding. MW = molecular weight. Gallbladder (g.b.) values are from this paper; "nerve", from Hille's (1971) measurements on the Na^+ channel of myelinated nerve; and the four carriers in the last four columns and gramicidin, from Eisenman's and Krasne's (1973) and Krasne and Eisenman's (*personal communication*) measurements on glyceryl dioleate bilayers doped with the given antibiotic. Because valinomycin and the actins have relatively high P_K/P_{Na} and P_{NH_4}/P_{Na} values, respectively, and are therefore sensitive to trace contaminants of K^+ and NH_4^+, respectively, only upper bounds can be set on some of their P_X/P_{Na} values.

some of the differences between systems in permeability sequences of equally proton-rich cations (*see also* footnote 6, p. 249).

Another factor that may contribute to differences in permeability sequences is differences in sites, either in their electrostatic field strength, or in other forces contributing to overall strength of hydrogen bonds, or in coordination number. Just as Eisenman (1961, 1962, 1965*b*) showed that Eq. (7) predicts different selectivity sequences for inorganic cations as a function of site strength, so one also expects differences in nitrogenous cation permeability sequences as a function of site field strength. The empirically observed dependence of nitrogenous cation P_X/P_K values on P_{Na}/P_K values in gallbladder (Fig. 5) and in glass electrodes (Fig. 39 of Eisenman, 1965*a*) presumably arises from such a variation in field strength.

The remaining obvious difference between gallbladder and the other systems is quantitative: the *range* of selectivity is much narrower in gallbladder. Thus, the relative permeability coefficients of NH_4^+, $H_3C-NH_3^+$, $(H_3C)_2NH_2^+$, and $(H_3C)_3NH^+$, respectively, are 1.00, 0.47, 0.20, $\leqq 0.01$ in frog gallbladder; 1.00, 0.32, 0.07, $\leqq 0.01$ in rabbit gallbladder; 1.00, 0.0088, 0.00075, 0.000125 in valinomycin-doped bilayers; and 1.00, 0.0013, 0.00001, and 0.000004 in nonactin-doped bilayers. Relative permeability coefficients for 17 nitrogenous cations in rabbit gallbladder and in nerve (Table 8) exhibit no differences in sequence except for the relative positions of NH_4^+ and $H_2N-NH_3^+$. The major difference between rabbit gallbladder and nerve is that P_X/P_{Na} values fall within a measurable range ($P_X/P_{Na} >$ ca. 0.01) for only 6 of the 17 cations in nerve but for 14 of the 17 cations in rabbit gallbladder. These quantitative differences between gallbladder and other systems, in their range of selectivity for nitrogenous cations, are entirely analogous to the same type of differences noted previously for inorganic cations (Barry *et al.*, 1971; Moreno & Diamond, 1974*b*, Fig. 14). For example, the alkali cation selectivity sequence of gallbladder is similar to that of some glass electrodes, some carrier-doped bilayers, and nerve's K^+ channel, but the range of selectivity is at least an order of magnitude narrower in gallbladder. Analogous quantitative differences in model systems (Eisenman, 1962, Fig. 18) suggest as an interpretation that the permeation channel through gallbladder tight junction is more hydrated than in glass or the other systems compared. This conclusion is in accord with other knowledge about tight junctions. The low selectivity and high hydration of ion-selective channels in gallbladder tight junctions may be due to their relatively wide pore (estimated from the analysis of steric restriction) as compared to the narrower values of pore radius estimated for the K^+

channel and Na^+ channel of nerve (Hille, 1971, 1973; Benzanilla & Armstrong, 1972), or as compared to the known cavity or channel sizes of the carriers and channel-formers listed in Table 7. While the estimate of gallbladder equivalent pore radius is based in too many assumptions to merit stress (p. 224), it is still interesting to note that a cross-section of the equivalent pore would admit at least three water molecules in rabbit (more than three in frog) in addition to a small ion. In contrast, the K^+ and Na^+ channels of nerve have been estimated to admit not more than one water molecule in addition to the ion (Hille, 1971, 1973).

These striking quantitative differences in range of selectivity between gallbladder and other systems are paralleled by much less striking differences among gallbladders of different species. Fig. 10 shows that P_X/P_{Na} ratios for nitrogenous cations cover a narrower range in frog gallbladder than in rabbit gallbladder, after correction for the steric effect. Fig. 12 shows that each donor proton increases P_X/P_{Na} by a larger factor in rabbit gallbladder than in frog gallbladder. Since the equivalent pore radius calculated from the steric effect is wider in frog gallbladder than in rabbit gallbladder, it is natural to attribute this species difference to the same cause as that postulated for the larger difference between gallbladder and other systems – viz., that the permeation channel is more hydrated in frog gallbladder (because of its wider radius) than in rabbit gallbladder. Higher hydration in a channel, or incomplete dehydration of an ion at a site, means that the terms $\Delta F_{ion/site}$ and $\Delta F_{hydration}$ in Eq. (7) are reduced, thereby reducing the absolute magnitude of their difference, hence of $\Delta F_{transfer}$ and of permeability ratios. A narrow pore may further mean that a small cation can fit in the pore together with a water molecule, but a larger cation can fit only in the absence of water, thereby altering the cations' relative permeabilities. Alternatively, Fig. 12 could mean that the proton-acceptor sites of rabbit gallbladder form stronger H-bonds than do those of frog gallbladder. To express this interpretation quantitatively, note from Eq. (7) that if values of u and of u^* (after correcting for steric restriction) are proportional (*cf.* p. 241), the slope of Fig. 12 would equal $-\Delta F_{transfer}(H)/2.303\,RT\,(P_{Na}/u^*_{Na})$, where $\Delta F_{transfer}(H)$ refers to the difference between the strength of an H-bond formed by a proton donor with the membrane site and with water. From the slopes of Fig. 12, one would then calculate that an H-bond with a frog gallbladder or rabbit gallbladder site is 92 or 403 cal/mole stronger, respectively, than an H-bond with water.

Thus, nitrogenous cation selectivity patterns in gallbladder, nerve, and several carriers correlate in the first instance with the cations' proton-donor ability, suggesting that these systems have proton-acceptor sites that distin-

guish more sharply among proton donors than does water.[6] Qualitative differences between these systems in permeability sequence may reflect differences in steric restriction, differences in site field strength or in proton-acceptor strength (which in turn depends partly on field strength), differences in coordination number, or other factors. Until a theoretical treatment that can predict nitrogenous cation selectivity sequences as a function of these variables has been achieved, it will remain difficult to account more exactly for details of nitrogenous cation permeability sequences. Quantitative differences between these systems in their ranges of permeability ratios probably reflect differences in hydration.

The close similarity in nitrogenous cation permeability sequence between rabbit gallbladder and the Na^+ channel of nerve (Table 8) makes it probable that the same explanation of nitrogenous cation selectivity will be found to apply to both systems. Since Figs. 8 and 12 suggest strongly that permeability differences in gallbladder are related to differences in proton donor ability (as directly affecting the energy of site/solute interactions) and to differences in steric restriction, we assume that both of these factors are also important in nerve. The importance of size considerations was recognized by Hille (1971, p. 613) in his pioneer studies on organic cation selectivity in nerve. In particular, Hille noted that a proton-rich solute which behaved as if it were the larger solute in a non-H-bonding environment behaved as if it were the smaller solute in a proton-acceptor environment. Thus, Hille reasoned that hydrogen bonding should affect the magnitude of steric restriction on a solute, in agreement with the evidence from numerous examples in gallbladder.

However, Hille (1971, p. 613) reasoned against the energy of hydrogen bonding contributing directly (i.e., via effects on site/solute forces, and independently of steric restrictions) to permeability differences, as we have proposed. Hille's reasons for rejecting this interpretation were two-fold. First, he argued that a channel is unlikely to be able to offer as concentrated a hydrogen bonding environment as water provides, so that a solute's ability to form hydrogen bonds should retard rather than promote permeation. This argument has already been discussed on pp. 241–242. Second, Hille noted that $H_3C-NH-NH_3^+$, $H_2N-C(CH_3)=NH_2^+$, and $H_3C-NH-C(NH_2)=NH_2^+$ are impermeant in nerve despite being able to make

6 Naturally, proton-acceptor sites could distinguish *less* sharply among proton donor than does water. If such sites were controlling the permeability of a membrane, they would yield a selectivity pattern opposite to that observed in gallbladder: permeability would *decrease* with increasing proton-donor ability. The carrier hexadecavalinomycin does exhibit such a pattern (Table 7).

Table 8. Comparison of organic cation permeabilities in the Na^+ channel of nerve (from Hille, 1971) and in rabbit gallbladder

Solute	P_X/P_{Na}, nerve	P_X/P_{Na}, rabbit gallbladder
$HO-NH_3^+$	0.94	1.63
$H_2N-NH_3^+$	0.59	1.05
NH_4^+	0.16	1.42
$H_2N=CH-NH_2^+$	0.14	1.03
$(H_2N)_2C=NH_2$	0.13	0.70
$H_2N-NH-C(NH_2)=NH_2^+$	0.06	0.57
$H_3C-NH_3^+$	~0	0.46
$H_3C-NH-NH_3^+$	~0	0.30
$H_2N-NH^+=C(NH-NH_2)_2$	~0	0.28
$CH=CH-NH-CH=NH^+$	~0	0.28
$H_3C-NH-C(NH_2)=NH_2^+$	~0	0.26
$H_2N-C(CH_3)=NH_2^+$	~0	0.19
$H_3C-NH_2^+-CH_3$	~0	0.09
$HN=C(NH_2)-NH-C(NH_2)=NH_2^+$	~0	0.07
$(H_3C)_4N^+$	~0	~0
$(H_3C-CH_2)_4N^+$	~0	~0
$(H_3C)_3N^+-CH_2-CH_2-OH$	~0	~0

many H-bonds. Table 8 shows that their relative positions in the nerve permeability sequence are consistent with their positions in the gallbladder permeability sequence, but the actual P_X/P_{Na} values in nerve are too low to measure because of nerve's greater range of selectivity. The actual P_X/P_{Na} values in gallbladder fall close to the pattern defined by other solutes with $\geqq 4$ donor protons; i.e., their P_X/P_{Na} values are as one would expect from their H-bonding ability and their large size or low u_X/u_{Na} values.

Thus, Hille's measurements of organic cation selectivity in nerve suggest to us that permeability differences in nerve arise both from H-bonding to sites and from steric effects, as in gallbladder. As discussed on p. 243, it seems that estimation of a pore size for the Na^+ channel of nerve, from permeability differences attributed to steric effects, requires consideration also of permeability differences arising from H-bonding.

Implications for Alkali Cation Selectivity

We showed previously that alkali cation selectivity depends upon site field strength and steric restriction; that equivalent cylindrical pore radii estimated from the steric effect on alkali cations are ca. 4 Å in rabbit gallbladder and 6 Å in frog gallbladder; that cation permeation is controlled

Table 9. Steric effect on metallic cation and NH_4^+ permeability in gallbladder

Cation	P_X/P_{Na}			
	Rabbit		Frog	
	uncorrected	corrected	uncorrected	corrected
Li^+	0.90 ± 0.02	0.64	0.59 ± 0.04	0.50
Na^+	1.0	1.0	1.0	1.0
K^+	1.92 ± 0.04	3.07	1.43 ± 0.06	1.76
Tl^+	1.81 ± 0.19	3.38	1.81 ± 0.09	2.39
Rb^+	1.46 ± 0.03	2.92	1.47 ± 0.06	2.00
NH_4^+	1.42 ± 0.08	3.23	1.66 ± 0.09	2.48
Cs^+	0.58 ± 0.02	1.79	1.11 ± 0.06	1.81

Uncorrected values are from Moreno and Diamond, 1974*a*, Table 3. "Corrected" values have been corrected for effects of steric restriction, i.e., are $(P_X/P_{Na})'$ values calculated as described on p. 227.

by acidic groups with a pK_a value near 4.5; and that the permeation channel is relatively highly hydrated (Moreno & Diamond, 1974*b*). The present study confirms the conclusion of high hydration. Our new radius estimate based on nitrogenous cations has been able to use many more cations than did our previous estimate based on seven inorganic cations alone, but the new estimate is close to the former one: 4.4 Å in rabbit gallbladder, 8.1 Å in frog gallbladder. The present study has yielded the new conclusions that the cation-binding sites are proton acceptors and can form up to four strong H-bonds with suitable proton donors. At least three independent lines of evidence now support this conclusion: the dependence of permeability coefficients on the solute's number of donor protons (Figs. 4, 11, 12); the dependence of the solute's effective molecular radius on number of donor protons (Figs. 7 and 8 and pp. 221–226); and the structure-activity relations of 2,4,6-triaminopyrimidine (TAP) and its derivatives in suppressing cation permeability (Moreno, 1975*a*).

"Raw" permeability coefficients of inorganic cations, uncorrected for the steric effect, were found to be in the sequence $Tl^+ > NH_4^+ > Rb^+$, $K^+ > Cs^+ > Na^+ > Li^+$ in frog gallbladder, K^+, $Tl^+ > Rb^+ > NH_4^+ > Na^+ > Li^+ > Cs^+$ in rabbit gallbladder (Moreno & Diamond, 1974*b*). Of the 11 alkali cation sequences that Eisenman (1961, 1962, 1965) predicted from considerations of field strength, the "raw" frog sequence was on the borderline between Eisenman's sequences III and IV, while the rabbit sequence differed from Eisenman's sequence V only in the reversed positions of Cs^+ and Li^+, presumed due to steric restrictions on the large Cs^+

cation. We have now corrected our previous estimates (Moreno & Diamond, 1974*b*, Table 3) of alkali cation permeability coefficients for the steric effect, by the same method used to obtain the corrected permeability coefficients for nitrogenous cations presented in Fig. 9. As seen in Table 9, the corrected sequence in the frog is $Rb^+ > Cs^+ > K^+ > Na^+ > Li^+$ (Eisenman's sequence II), while the sequence in the rabbit is $K^+ \geqq Rb^+ > Cs^+ > Na^+ > Li^+$ (Eisenman's sequence IV). Thus, the steric effect does account for the discrepancy between the rabbit sequence and Eisenman's set of predicted sequences, as suspected previously. The range of permeability coefficients from the least to the most permeant alkali cation is increased by the steric correction from a factor of 3.1 to 5.6 in frog gallbladder, and from 2.1 to 5.9 in rabbit gallbladder. These calculations emphasize again that both field strength and steric restriction contribute to alkali cation selectivity.

This work was supported by grant GM 14772 and Peptic Ulcer Center grant AM 17328, and by an International Postdoctoral Fellowship (awarded to J.H.M.) from the National Institutes of Health. It is a pleasure to record our debt to Drs. G. Eisenman and S. Krasne for discussion of the project and suggestions on the manuscript.

Appendix

Free-solution Mobilities of Nitrogenous Cations

Since values of the free-solution mobility u_X were unavailable for most nitrogenous cations, we measured u_X for all cations studied except four.

Measurements. The equivalent conductance $\Lambda_{X\mathrm{Cl}}$ of a chloride solution of each cation was measured at 25.0 ± 0.1 °C, at a concentration of approximately 150 mM (i.e., close to that of our experimental solution), and at a pH such that more than 99 % of the cation was in the charged form (generally pH 7; cations with low pK_a's were studied at a lower pH). We used a conductivity cell with platinized platinum electrodes, determined the cell constant with KCl standard solutions, and measured Λ with alternating currents (1000 Hz) and a Wheatstone bridge (General Radio, Mass.). Each solution was measured three times. The three values generally agreed to within 0.15 %. As a check on accuracy we measured Λ of 200 mM NaCl and obtained 101.87 cm^2/ohm equivalent, close to the accepted value of 101.71 (MacInnes, 1961; Robinson & Stokes, 1970).

Calculations. The cation equivalent conductance in an XCl solution, $\Lambda_{X^+}^{X\mathrm{Cl}}$, was calculated from the measured $\Lambda_{X\mathrm{Cl}}$ by the equation

$$\Lambda_{X\mathrm{Cl}} = \Lambda_{X^+}^{X\mathrm{Cl}} + \Lambda_{\mathrm{Cl}^-}^{X\mathrm{Cl}} \tag{A.1}$$

making the assumption that Λ_{Cl^-} has the same value in an XCl solution as in a KCl solution at the same concentration:

$$\Lambda_{Cl^-}^{XCl} = \Lambda_{Cl^-}^{KCl}. \tag{A.2}$$

$\Lambda_{Cl^-}^{KCl}$ is calculated from published values of Λ_{KCl} and the transport number $t_{Cl^-}^{KCl}$ (Robinson & Stokes, 1970), as 64.52 cm^2/ohm equivalent at 150 mM. Then u_X/u_{Na} is calculated as

$$u_X/u_{Na} = \Lambda_{X^+}^{XCl}/\Lambda_{Na^+}^{NaCl} \tag{A.3}$$

taking $\Lambda_{Na^+}^{NaCl}$ as 39.87 cm^2/ohm equivalent at 150 mM (Robinson & Stokes, 1970). Table 4, column 5, gives the resulting values of u_X/u_{Na}.

Eq. (A.2) is strictly valid only in the limit of infinite dilution. The error introduced by assuming validity of Eq. (A.2) at 150 mM was assessed in three ways:

1. For NH_4Cl, KCl, NaCl, LiCl, and HCl, Λ_{XCl} and t_{Cl}^{XCl} at 100 mM have been measured (MacInnes, 1961; Robinson & Stokes, 1970), so that $\Lambda_{Cl^-}^{XCl}$ at 100 mM may be calculated. Values of $\Lambda_{Cl^-}^{XCl}$ for all five salts fall between 65.492 and 65.977 cm^2/ohm equivalent; i.e., Eq. (A.2) is a good approximation. (Note that this does not imply anything about how close $\Lambda_{Cl^-}^{XCl}$ at 100 mM is to $\Lambda_{Cl^-}^{XCl}$ at infinite dilution. For these same five salts, this difference ranges up to 3% of the value of $\Lambda_{Cl^-}^{XCl}$ at 100 mM.)

2. Our value of $\Lambda_{NH^+}^{NH_4Cl}$, calculated on the assumption that Eq. (A.2) is valid, yields a value of $t_{NH^+}^{NH_4Cl} = 0.496$ at 150 mM. The measured value at this concentration is 0.491 (MacInnes, 1961).

3. In the cases of two salts, $H_3CCH_2NH_3^+Cl^-$ and $H_3C(CH_2)_5NH_3^+Cl^-$, we also determined u_X/u_{Cl} by a different technique that does not assume the validity of Eq. (A.2). This technique involved measuring the junction potential between 100 and 200 mM solutions of the salt, using the circuit Ag/AgCl electrode |100 mM X^+Cl^- solution| 100 mM X^+Cl^- agar-immobilized bridge |200 mM X^+Cl^- solution| Ag/AgCl electrode. The calculation of u_X/u_{Cl} from the measured junction potential assumes that the activity coefficient γ_{X^+} equals γ_{Na^+} in a NaCl solution at the same concentration, and that the Guggenheim assumption $\gamma_{X^+} = \gamma_{Cl^-}$ holds (*see* Barry & Diamond, 1970, for details). The resulting values of u_X/u_{Cl} from conductance measurements and from junction potential measurements, respectively, were: for $H_3CCH_2NH_3^+Cl^-$, 0.515 and 0.518; for $H_3C(CH_2)_5NH_3^+Cl^-$, 0.274 and 0.268. Despite the different assumptions of the two methods, the agreement for each salt is good.

Table A.1. Comparison of Λ_{X^+} values measured by us and by Desnoyers *et al.* (1969)

Salt	Desnoyers *et al.* (1969)		Present study
	$\Lambda_{X\,Br}$	Λ_{X^+}	Λ_{X^+}
$NH_4^+Br^-$	129.4	63.3	63.6
$CH_3-NH_3^+Br^-$	111.7	45.7	45.6
$CH_3-CH_2-NH_3^+Br^-$	99.81	33.7	33.2
$CH_3-(CH_2)_2-NH_3^+Br^-$	94.04	28.0	28.5
$CH_3-(CH_2)_3-NH_3^+Br^-$	89.96	23.9	23.3
$CH_3-(CH_2)_4-NH_3^+Br^-$	86.24	20.2	—
$CH_3-(CH_2)_5-NH_3^+Br^+$	83.92	17.8	17.7
$CH_3-(CH_2)_6-NH_3^+Br^-$	81.94	15.9	—

Units of Λ values are cm^2/ohm equivalent. Values of Λ_{X^+} are extracted from measurements by Desnoyers *et al.* (1969) on XBr solutions and by us on XCl solutions. Note the good agreement between the resulting values of Λ_{X^+} (columns 3 and 4).

Comparison of our Results with Published Data. Physical chemists are more interested in values of Λ° (the equivalent conductance at infinite dilution) than of Λ at finite concentrations, since the former values are simpler to interpret. To our knowledge, the only systematic published study of nitrogenous cation Λ's at high concentrations is by Desnoyers, Arel and Leduc (1969), who measured conductances of *n*-alkylammonium bromide salts at various concentrations. They found that Λ was empirically related to concentration C by an equation of the form

$$\Lambda = \Lambda^\circ - A\sqrt{C} + BC \tag{A.4}$$

where A and B are fitted constants for each salt. Table A.1, column 2, gives $\Lambda_{X\,Br}$ values at 150 mM calculated from this equation. In analogy to Eq.(A.2) we assume that $\Lambda_{Br^-}^{X\,Br} = \Lambda_{Br^-}^{X\,Br}$ and calculate $\Lambda_{Br^-} = \Lambda_{KBr}\, t_{Br^-}^{KBr} = 66.09$ cm^2/ohm equivalent at 150 mM, from published values of Λ_{KBr} and $t_{Br^-}^{KBr}$ (MacInnes, 1961; Robinson & Stokes, 1970). Subtracting this value of Λ_{Br^-} from the $\Lambda_{X\,Br}$ values of column 2 gives the Λ_{X^+} values of column 3 obtained from the data of Desnoyers *et al.* (1969). Column 4 gives the Λ_{X^+} values obtained from our measurements. The two sets of measurements differ in that Eq. (A.2) is applied to Λ_{Cl^-} in one case and to Λ_{Br^-} in the other case, and in that our values of Λ at 150 mM were measured whereas those of Desnoyers *et al.* are interpolated by means of Eq. (A.4) from measurements at other concentrations. The agreement between the two sets of data is good.

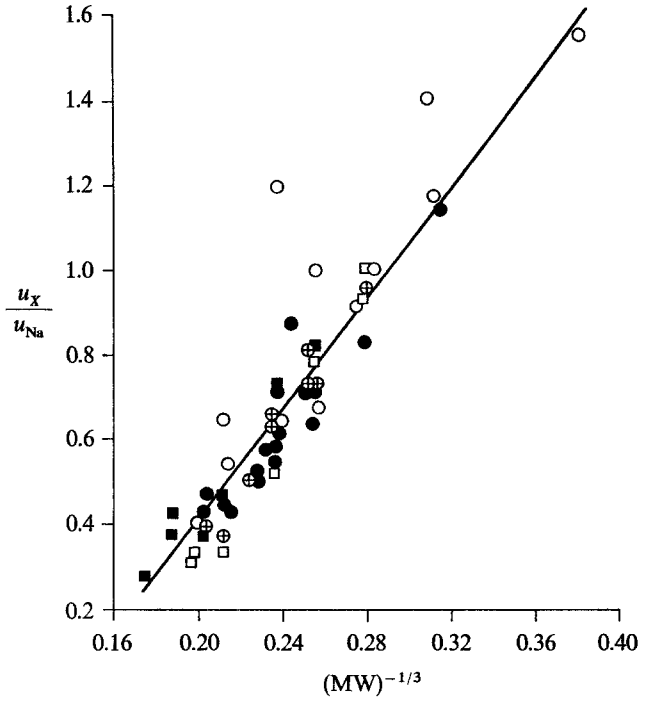

Fig. 16. Free-solution mobility ratios u_X/u_{Na} of nitrogenous cations X^+ in 150 mM X^+Cl^- solutions at 23 °C, as a function of $(MW)^{-1/3}$. Symbols as in Fig. 2. Note that u_X/u_{Na} is inversely proportional to $(MW)^{-1/3}$. The line traced through the points is the regression line $u_X/u_{Na} = -0.9 + 6.54\,(MW)^{-1/3}$ (regression coefficient = 0.91)

Interpretation of Results. Fig. 16 displays our u_X/u_{Na} values as a function of $\sqrt[3]{(MW)}$, to permit comparison with predictions from the Stokes-Einstein equation. This equation, which should apply at infinite dilution to solute molecules that are much larger than the solvent molecules, reads:

$$D_{12} = kT/6\pi\eta_1 r_2 \tag{A.5}$$

or

$$D_{12} = kT/f_{12}\eta_1 r_2 \tag{A.6}$$

where subscripts 1 and 2 refer to solvent and solute, respectively, D_{12} is the solute's diffusion coefficient, k the Boltzmann constant, T absolute temperature, η_1 solvent viscosity, r_2 solute radius, and f_{12} a frictional coefficient. The molecular radius is that of the effectively diffusing particle, including not only the solute molecule itself but also water molecules within the surface of shear or "water of hydration". Eq. (A.5) gives a good fit to measured diffusion coefficients for large solute molecules in water, taking $\sqrt[3]{MW}$ as a measure of r_2.

Fig. 16 shows that Eq. (A.5) gives a fairly good fit to the measured cation mobilities, and that deviations related to the different number of H-bonds formed between different solutes and water are not enormous. This is initially surprising: one might have expected increasing numbers of H-bonds to mean more tightly bound and more numerous hydrated water molecules, hence the ratio of effective diffusing volume to anhydrous volume to be a marked function of H-bonding ability. We interpret our results in term of the explanation provided by Horowitz and Fenichel (1964; *also* Fenichel & Horowitz, 1965) for a similar pattern in aqueous diffusion coefficients of nonelectrolytes. They measured nonelectrolyte D's in water and in another hydrogen-bonding solvent, formamide. In formamide, as initially expected, f_{12} of Eq. (A.6) increased, and D_{12} decreased, with increasing number and strength of H-bonding groups on the solute. In water these relations were much weaker. Horowitz and Fenichel pointed out that not only does water, like formamide, make H-bonds with H-bonding solutes: water also, unlike formamide, interacts with non-H-bonding groups by "hydrophobic hydration" or "iceberg formation" (*see* Frank & Evans, 1945, for discussion), which probably tends to immobilize the moving particle or increase its effective volume in the same way as do solute-solvent H-bonds. Since the proportions of H-bonding groups and non-H-bonding groups vary reciprocally in a molecule, their effects tend to cancel in water (but not in formamide). In addition, solutes that form a large number of H-bonds, such as urea and guanidine, have a "structure-breaking" effect on water (Rupley, 1964). This may explain the deviantly somewhat high values of Λ_{X^+} in Fig. 16 for guanidine, aminoguanidine, and triaminoguanidine, which have $n_H = 6 - 9$.

References

Adams, J. M., Small, R. W. H. 1973. The structure of ammonium carbamate. *Acta Crystalographica* **B29**:2317

Armstrong, C. M., Binstock, L. J. 1965. Anomalous rectification in the squid giant axon injected with tetraethylammonium chloride. *J. Gen. Physiol.* **48**:859

Barry, P. H., Diamond, J. M. 1970. Junction potentials, electrode standard potentials, and other problems in interpreting electrical properties of membranes. *J. Membrane Biol.* **3**:93

Barry, P. H., Diamond, J. M., Wright, E. M. 1971. The mechanism of cation permeation in rabbit gallbladder. Dilution potentials and biionic potentials. *J. Membrane Biol.* **4**:358

Benzanilla, F., Armstrong, C. M. 1972. Negative conductance caused by entry of sodium and cesium ions into the potassium channels of squid axons. *J. Gen. Physiol.* **60**:588

Collander, R. 1949. Die Verteilung organischer Verbindungen zwischen Äther und Wasser. *Acta Chem. Scand.* **4**:1085

Collander, R. 1954. The permeability of *Nitella* to non-electrolytes. *Physiol. Pl.* **7**:420

Desnoyers, J. E., Arel, M., Leduc, P. A. 1969. Conductance and viscosity of *n*-alkylamine hydrobromides in water at 25 °C. *Canad. J. Chem.* **47**:547

Diamond, J. M. 1962. Mechanism of solute transport by the gall-bladder. *J. Physiol.* **161**:474

Diamond, J. M. 1966. A rapid method for determining voltage-concentration relations across membranes. *J. Physiol.* **183**:83

Diamond, J. M., Katz, Y. 1974. Interpretation of nonelectrolyte partition coefficients between dimyristoyl lecithin and water. *J. Membrane Biol.* **17**:121

Diamond, J. M., Wright, E. M. 1969*a*. Biological membranes: The physical basis of ion and non-electrolyte selectivity. *Annu. Rev. Physiol.* **31**:581

Diamond, J. M., Wright, E. M. 1969*b*. Molecular forces governing non-electrolyte permeation through cell membranes. *Proc. Roy. Soc. B. (London)* **172**:273

Eisenman, G. 1961. On the elementary atomic origin of equilibrium ionic specificity. *In:* Symposium on Membrane Transport and Metabolism. A. Kleinzeller and A. Kotyk, editors. p. 163. Academic Press Inc., New York

Eisenman, G. 1962. Cation selective glass electrodes and their mode of operation. *Biophys. J.*, Part 2. **2**:259

Eisenman, G. 1965*a*. The electrochemistry of cation-sensitive glass electrodes. *In:* Advances in Analytical Chemistry and Instrumentation. C. N. Reilley, editor. p. 215. Wiley-Interscience, New York

Eisenman, G. 1965*b*. Some elementary factors involved in specific ion permeation. *Proc. XXIII Int. Congr. Physiol. Sci.*, Tokyo, p. 489

Eisenman, G., Krasne, S. J. 1973. The selectivity of carrier antibiotics for substituted ammonium ions. *Biophys. J.* **13**:244a

Eisenman, G., Krasne, S. J. 1974. The ion selectivity of carrier molecules, membranes and enzymes. *In:* MTP International Review of Science, Biochemical Series. C. F. Fox, editor. Vol. 2. Butterworths, London

Fenichel, I. R., Horowitz, S. B. 1965. Diffusional specificity of water. *Ann. N. Y. Acad. Sci.* **125**:290

Finkelstein, A. 1970. Weak acid uncouplers of oxidative phosphorylation. Mechanism of action on thin lipid membranes. *Biochim. Biophys. Acta* **205**:1

Frank, H. S., Evans, M. W. 1945. Free volume and entropy in condensed systems. III. Entropy in dilute solutions; structure and thermodynamics in aqueous electrolytes. *J. Chem. Phys.* **13**:507

Frömter, E. 1972. The route of passive ion movement through the epithelium of *Necturus* gallbladder. *J. Membrane Biol.* **8**:259

Frömter, E., Diamond, J. M. 1972. Route of passive ion permeation in epithelia. *Nature, New Biol.* **235**:9

Galey, W. R., Owen, J. D., Solomon, A. R. 1973. Temperature dependance of non-electrolyte permeation across red cell membranes. *J. Gen. Physiol.* **61**:727

Garbassi, F., Giarda, L., Fagherazzi, G. 1972. The crystal structure of methyl diammonium phosphate dihydrate. *Acta Crystalographica.* **B28**:1663

Hadzi, D., editor. 1959. Hydrogen Bonding. Pergamon Press, New York

Hille, B. 1967. The selective inhibition of delayed potassium currents in nerve by tetraethylammonium ion. *J. Gen. Physiol.* **50**:1287

Hille, B. 1971. The permeability of the sodium channel to organic cations in myelinated nerve. *J. Gen. Physiol.* **58**:599

Hille, B. 1973. Potassium channels in myelinated nerve: Selective permeability to small cations. *J. Gen. Physiol.* **61**:669

Hille, B. 1975. Ionic selectivity of Na and K channels of nerve membranes. *In:* Membranes—A Series of Advances. G. Eisenman, editor. Vol. 3. Marcel Dekker, New York

Hingson, D. J., Diamond, J. M. 1972. Comparison of nonelectrolyte permeability patterns in several epithelia. *J. Membrane Biol.* **10**:93

Horowitz, S. B., Fenichel, I. R. 1964. Solute diffusional specificity in hydrogen-bonding systems. *J. Physical Chem.* **68**:3378

Kielland, J. 1937. Individual activity coefficients of ions in aqueous solutions. *J. Amer. Chem. Soc.* **59**:1675

Krasne, S. J., Eisenman, G. 1973. Molecular basis of ion selectivity. *In:* Membranes—A Series of Advances. G. Eisenman, editor. Vol. 2, Chap. 3, Sec. V. Marcel Dekker, New York

Krishnan, C. V., Friedman, H. L. 1970. Enthalpies of alkylammonium ions in water, heavy-water, propylene carbonate and dimethylsulfoxide. *J. Phys. Chem.* **74**:3900

Ladd, M. F. C. 1968. The radii of spherical ions. *Theoret. Chem. Acta (Berl.)* **12**:333

Lange, Y., Gary-Bobo, C. M., Solomon, A. K. 1974. Nonelectrolyte diffusion through lecithin-water lamellar phases and red cell membranes. *J. Gen. Physiol. (in press)*

LeBlanc, O. H., Jr. 1971. The effect of uncouplers of oxydative phosphorylation on lipid bilayer membranes: Carbonylcyanide *m*-chlorophenylhydrazone. *J. Membrane Biol.* **4**:227

Liberman, E. A., Topaly, V. P. 1968. Transfer of ions across bimolecular membranes and classification of uncouplers of oxidative phosphorylation. *Biofizika* **13**:1025

Lindenbaum, S., Boyd, G. E. 1964. Osmotic and activity coefficients for the symmetrical tetraalkylammonium halides in aqueous solution at 25 °C. *J. Phys. Chem.* **68**:911

Lorente de Nó, R., Vidal, F., Larramendi, L. M. H. 1957. Restoration of sodium-deficient frog nerve fibers by onium ions. *Nature* **179**:737

MacInnes, D. A. 1961. The Principles of Electrochemistry. Dover Publications Inc., New York

Maeno, T. 1974. Studies on the permeability of end-plate membrane to several organic cations. *J. Physiol. Soc. Japan* **36**:89

Moreno, J. H. 1974. Blockage of cation permeability across the tight junctions of gallbladder and other leaky epithelia. *Nature* **251**:150

Moreno, J. H. 1975*a*. The blockage of gallbladder tight junction cation selective channels by 2,4,6-triaminopyrimidinium (TAP). *J. Gen. Physiol. (submitted)*

Moreno, J. H. 1975*b*. The active salt transport and the routes of nonelectrolyte permeability in gallbladder: Effect of 2,4,6-triaminopyrimidinium (TAP). *J. Gen. Physiol. (submitted)*

Moreno, J. H., Diamond, J. M. 1973*a*. Selective permeation of small organic cations in gallbladder epithelium. *Biophys. J.* **13**:85a

Moreno, J. H., Diamond, J. M. 1973*b*. Selectivity isotherms for permeation of monovalent cations in gallbladder epithelium. *Nature, New Biol.* **246**:92

Moreno, J. H., Diamond, J. M. 1974*a*. Role of hydrogen bonding in organic cation discrimination by "tight junctions" of gallbladder epithelium. *Nature* **247**:368

Moreno, J. H., Diamond, J. M. 1974*b*. Discrimination of monovalent inorganic cations by "tight" junctions of gallbladder epithelium. *J. Membrane Biol.* **15**:277

Moreno, J. H., Diamond, J. M. 1975. Cation permeation mechanism and cation selectivity in "tight junctions" of gallbladder epithelium. *In:* Membranes—A Series of Advances. G. Eisenman, editor. Vol. 3. Marcel Dekker, New York *(in press)*

Naccache, P., Sha'afi, R. I. 1973. Patterns of nonelectrolyte permeability in human red blood cell membrane. *J. Gen. Physiol.* **62**:714

Parlin, R. B., Eyring, H. 1957. Membrane permeability and electrical potential. *In:* Ion Transport across Membranes. H. T. Clarke, editor. Academic Press, New York

Pauling, L. 1960. The Nature of the Chemical Bond. Cornell University Press, Ithaca, N.Y.

Pimentel, G. C., McClellan, A. L. 1960. The Hydrogen Bond. Reinhold Publishing Corp., New York

Renkin, E. M. 1954. Filtration, diffusion, and molecular sieving through porous cellulose membranes. *J. Gen. Physiol.* **38**:225

Robinson, R. A., Stokes, R. H. 1970. Electrolyte Solutions. Butterworths, London

Rupley, J. A. 1964. The effect of urea and amides upon water structure. *J. Phys. Chem.* **68**:2002

Sanderson, P. H. 1952. Potentiometric determination of chloride in biological fluids. *Biochem. J.* **52**:502

Sherry, H. S. 1969. The ion-exchange properties of zeolites. *In:* Ion Exchange. J. Marinsky, editor. Vol. 2, p. 89. Marcel Dekker, New York

Simon, W., Morf, W. E. 1973. Alkali cation specificity of carrier antibiotics and their behavior in bulk membranes. *In:* Membranes—A Series of Advances. G. Eisenman, editor. Vol. 2, p. 329. Marcel Dekker, New York

Smulders, A. P., Wright, E. M. 1971. The magnitude of nonelectrolyte selectivity in the gallbladder epithelium. *J. Membrane Biol.* **5**:297

Tasaki, I., Hagiwara, S. 1957. Demonstration of two stable potential states in the squid giant axon under tetraethylammonium chloride. *J. Gen. Physiol.* **40**:859

Tedeschi, H., Harris, D. L. 1955. The osmotic behavior and permeability to nonelectrolytes of mitochondria. *Arch. Biochem. Biophys.* **58**:52

Wartiovaara, V. 1942. Über die Temperaturabhängigkeit der Protoplasmapermeabilität. *Ann. Bot. Soc. Zool.-Bot. Fen. Vanamo.* **16**:1

Wartiovaara, V. 1956. Abhängigkeit des Stoffaustausches von der Temperatur. *In:* Handbuch der Pflanzenphysiologie. Vol. 2, p. 369. W. Ruhland, editor. Springer-Verlag, Berlin

Wright, E. M., Diamond, J. M. 1968. Effects of pH and polyvalent cations on the selective permeability of gall-bladder epithelium to monovalent ions. *Biochim. Biophys. Acta* **163**:57

Wright, E. M., Diamond, J. M. 1969. Patterns of non-electrolyte permeability. *Proc. Roy. Soc. B. (London)* **172**:227

Wright, E. M., Pietras, R. J. 1974. Routes of nonelectrolyte permeation across epithelial membranes. *J. Membrane Biol.* **17**:293

Wyckoff, R. W. G. 1962. Crystal Structures. John Wiley and Sons, New York